Can magnetic susceptibilities measured on outcrops be used for modelling (and constraining inversions of) aeromagnetic data?

by

William John McNeice

A thesis submitted in partial fulfillment
of the requirement for the degree of
Master of Science (MSc) in Geology

The Faculty of Graduate Studies
Laurentian University
Sudbury, Ontario, Canada

THESIS DEFENCE COMMITTEE/COMITÉ DE SOUTENANCE DE THÈSE
Laurentian Université/Université Laurentienne
Faculty of Graduate Studies/Faculté des études supérieures

Title of Thesis
Titre de la thèse: Can measured magnetic susceptibilities measured on outcrop be used for modeling (and constraining inversions of) acromagnetic data?

Name of Candidate
Nom du candidat: McNeice, William

Degree
Diplôme: Master of Science

Department/Program
Département/Programme: Geology

Date of Defence
Date de la soutenance: September 07, 2019

APPROVED/APPROUVÉ

Thesis Examiners/Examinateurs de thèse:

Dr. Richard Smith
(Supervisor/Directeur de thèse)

Dr. Esmaeil Eshaghi
(Committee member/Membre du comité)

Dr. Stephane Perrouty
(Committee member/Membre du comité)

Dr. Bernd Milkereit
(External Examiner/Examinateur externe)

Approved for the Faculty of Graduate Studies
Approuvé pour la Faculté des études supérieures
Dr. David Lesbarrères
Monsieur David Lesbarrères
Dean, Faculty of Graduate Studies
Doyen, Faculté des études supérieures

ACCESSIBILITY CLAUSE AND PERMISSION TO USE

Abstract

Magnetic susceptibilities measured on outcrop and drill-core samples using hand-held instruments have been shown in the literature to be useful for identifying mineralogical changes. It is not yet clear how useful these measurements are for constraining magnetic modelling and inversion. We have generated estimates of the apparent magnetic susceptibility of the ground by mathematical transformation of an aeromagnetic data and assumed that these values can be used to model the magnetic data. In the same area we have a large number of measurements on outcrop and have compared these two independent estimates. When the measured values are below $1x10^{-3}$ S.I., there is a no correlation between the measured and apparent values, interpreted to be likely due to the influence or interference from nearby or underlying magnetic sources. Hence, in this case the measured values cannot be used to constrain modelling and inversion. When the measurements are above this value there is a limited correlation, with values only agreeing to within a factor of about 10, so these values can be used as very rough constraints. The poor correlation is interpreted as due to the presence of remanent magnetization or heterogeneity of the magnetic susceptibility within the rock. A large database of outcrop measurements gives an indication of the range of the variation in magnetic susceptibility values that could be used in modelling.

Keywords

Abitibi greenstone belt, magnetic susceptibility, apparent magnetic susceptibility, Metal Earth project, modelling

Acknowledgment

Thank you Richard Smith and Esmaiel for helping me through to the end. Thank you Danielle Shirriff and Gary M^{c}Neice for your advice and support. There are many graduate students at Laurentian University that have helped me along the way, including but not limited to Amir Maleki, Fabiano Justina, Eric Roots, and Kendra Zammit.

TABLE OF CONTENTS

List of Figures

Figure Page

List of Tables

Table Page

CHAPTER 1

1 Introduction to Thesis

1.1 Introduction

The purpose of this chapter is to provide motivation for the study, and a description of the study location, geological setting, some theory, definitions. In addition, previous studies on the subject of magnetic susceptibility will be discussed.

There has been a recent interest in measuring the magnetic properties of outcrop and core samples (Smith, Shore, and Rainsford, 2012). These measurements have become practical because of the availability of hand-held field magnetic susceptibility meters, six of which have been reviewed by Deng and Smith (2016). These portable susceptibility meters are less commonly known as frequency shift meters, whereby the magnetic susceptibility of a sample can be determined when placed in an applied field from a coil sensor due to the effect the sample has on the operating frequency of the LC oscillator in the circuitry (Clark and Emerson, 1991). The measured values can be useful for a number of purposes. For example, if a mapping geologist or a core logger is using a magnetic susceptibility meter and identifies a change in the measured value, then this might indicate a geological change that could be indicative of changes in mineralogy, alteration (Berubé et al., 2018), metamorphism, and vein density (Byrne et al 2018). Similarly, changes in magnetic viscosity can be indicative of deformation (Gaucher and Smith, 2017).

Magnetic susceptibility can be measured in the field, on outcrop surfaces or samples, or in the laboratory using rock samples. This study uses data collected using portable magnetic susceptibility meters. There are several factors which can contribute to the quality of a

measurement when using a portable meter, such as the freshness of the sample face, the geometry of the rock face, and the conductivity of the sample (Muir, 2012).

These magnetic susceptibility measurements in combination with other measurements such as density, resistivity and gamma-ray spectrometry have also been used to classify the lithology, using a variety of machine learning algorithms (Mahmoodi and Smith, 2015; Mahmoodi et al., 2016; 2017; Berubé et al., 2018).

Susceptibility values can also be used by a geophysicist when modelling or inverting geophysical data to infer the subsurface geology of an area. However, since magnetic data are non-unique (Dentith and Mudge, 2014), the modelling and inversion are more successful if the magnetic properties of each material is known and there is a good understanding of the geology in any given study area (Lelièvre et al., 2009; Mahmoodi et al., 2017). The availability of geological information, magnetic susceptibility, and other rock properties is limited by the access to outcrops or drill core information. If there are outcrops available, then the magnetic susceptibility can be measured on the exposed rock, or a sample can be collected and the susceptibility (and remanence) can be measured in the laboratory (Clark and Emerson, 1991; Enkin et al., 2012). This study intends to assess how well these magnetic susceptibility measurements contribute to the modeling and, by extension, inversion processes. This is done by also estimating the magnetic susceptibility from high resolution aeromagnetic data by transforming the aeromagnetic data to an apparent susceptibility based on the method described by Bambrick et al., (1982). If it is assumed that the transformed magnetic susceptibility data are a representation of the magnetic susceptibilities that would explain the data, then the apparent susceptibilities estimated at a specific location should agree with the measured outcrop susceptibilities at the same location. This study uses data from an area where there are extensive outcrop measurements and high quality aeromagnetic grid data

that will be transformed to an apparent susceptibility using the Oasis Montaj software, version 9.6 (Geosoft Inc., 1997). Hence these two independent measurements can be compared.

I compare the two independent magnetic susceptibility measurements, by generating a cross-plot of these two quantities. Then I define a transect through a section of the study area and create a two dimensional (2D) model that is consistent with the mapped geology and the magnetic susceptibility measurements on outcrop. Any adjustments made to the susceptibilities of the model to ensure that the model data fit the measured aeromagnetic data should be consistent with the diversity of values measured on different lithologies and the susceptibilities estimated from aeromagnetic data.

1.2 Geological Setting and Study Location

The Abitibi greenstone belt (AGB) is the northeast portion of the Abitibi Wawa subprovince, located in the southeast of the Superior province, with rock ages between 2795 and 2670 Ma (Thurston et al., 2008). The Abitibi greenstone belt straddles the Ontario-Quebec border, extending 100s of kilometers eastward and westward into each province. The greenstone belt is generally composed of E-W trending successions of folded volcanic and sedimentary rocks with domes of intrusive rocks (Daigneault et al., 2004). The AGB can be broken down in to 6 different volcanic assemblages and 2 different sedimentary assemblages. The volcanic assemblages are, from the oldest, the Picaud (2750-2735 Ma), the Deloro (2734-2724 Ma), the Stoughton-Roquemaure (2723-2720 Ma), the Kidd-Munro (2720-2710 Ma), the Tisdale (2710-2704 Ma), and the Blake River (2704-2695 Ma); and the sedimentary assemblages are the Porcupine (2690-2685 Ma) and the Timiskaming (2679-2669 Ma) (Thurston et al., 2008; Monecke et al., 2017).

As of 2005, the AGB has been estimated to have produced approximately $120 billion in mineral production (Thurston et al., 2008). There are several large mining camps within the Abitibi greenstone belt, including the Timmins and Kirkland Lake-Larder Lake camps in Ontario, and the Rouyn-Noranda, Cadillac, Malartic, and Val-d'Or camps in Quebec. Each camp is situated along one of the two main deformation zones, the Porcupine-Destor fault zone and the Larder Lake-Cadillac fault zone (Monecke et al., 2017). Mines in the Abitibi are primarily exploited for gold, but there are many copper-zinc deposits, and several nickel-copper deposits.

The study area is an 85 km by 85 km area in Ontario bounded roughly by Highway 144 in the west and Highway 101 in the north, with the Timmins township situated in the northwest and the Matachewan township situated in the southeast corner. Figure 1 shows a geological map of the study area with these geographical reference points included. A section of the Porcupine-Destor fault zone is located in the north of the study area, and a section of the Larder Lake-Cadillac fault zone is located in the south. In the southern portion of the study area the belt is overlaid by younger Paleoproterozoic rocks of the Huronian Supergroup (Monecke et al., 2017), primarily composed of siltstone, sandstone, argillite, and conglomerate rocks. Many different Proterozoic dyke swarms are present throughout the study area, including but not limited to the 2446 to 2473 Ma Matachewan dyke swarm (Halls, Scott, and Davis, 2005), the 2167 to 2171 Ma Biscotasing dyke swarm (Halls, Scott, and Davis, 2005), the 1.2 Ga Sudbury dyke swarm (Krogh et al., 1987), and the 1140 Ma Abitibi dyke swarm (Krogh et al., 1987; OGS, 2011).

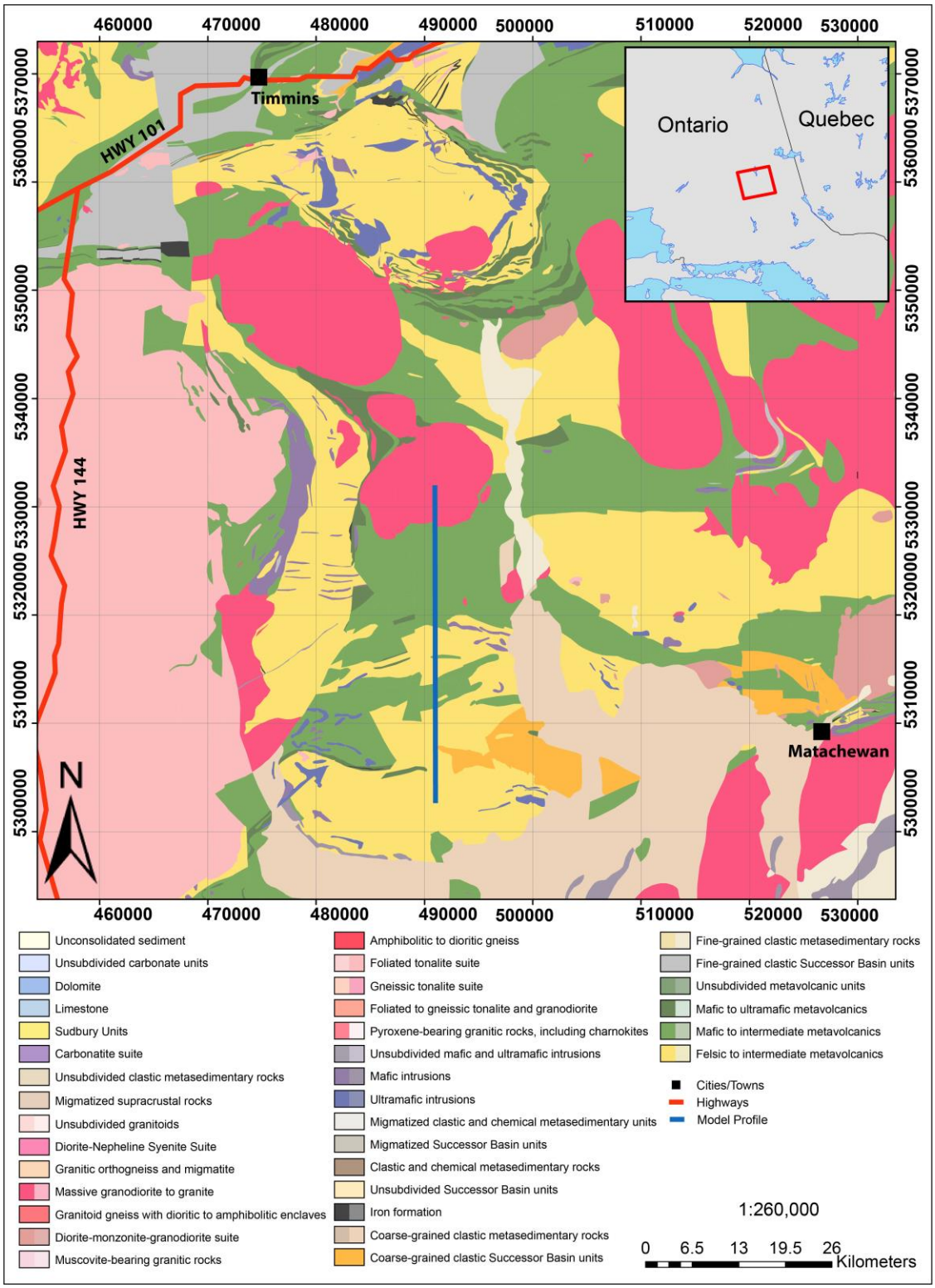

Figure 1 Geological map of the study area. The geological data was retrieved from OGS (2011). The location of diabase dykes has not been displayed on this map, but magnetic susceptibility information on diabase dykes are included in the susceptibility dataset.

1.3 Definitions and Theory

Magnetic susceptibility is a physical rock property that describes the ability of a material to exhibit a static induced magnetic field in the presence of an applied magnetic field (Dentith and Mudge, 2014). Magnetic susceptibility of a material can be represented mathematically (Clark, 1997) by the ratio between the induced field and the applied field (typically the geomagnetic field):

$$\kappa = \frac{\mathbf{M}}{\mathbf{H}} , \qquad (1)$$

where κ [unitless] represents the volume magnetic susceptibility, **H** [A/m] represents the applied field, and **M** [A/m] represents the induced static magnetic field. The induced and applied fields are vectors, but normally in the same direction, so κ is normally stated as a scalar. Volume magnetic susceptibility should not be confused with mass magnetic susceptibility (χ), which is derived by dividing the volume susceptibility by the density of the sample. For the duration of this study, the use of the term "magnetic susceptibility" and "susceptibility" will refer to volume magnetic susceptibility. The magnetic susceptibility can be defined using two different systems of units: the centimeter-gram-second (CGS) system and the international system of units (S.I.). Each system relies on a different definition of the permeability of free space, and a multiplication factor is required to convert between the two.

$$\kappa_{S.I.} = 4\pi\kappa_{CGS} \qquad (2)$$

Geological materials have susceptibilities which depend on the electron spins and the orbital motion of the electrons within that material (Dentith and Mudge, 2014). In the case when the

dipole moments align in the opposite direction to the applied field, the material is *diamagnetic*. Example diamagnetic minerals are quartz, calcite, feldspar, many clay minerals and water. For diamagnetic minerals, the susceptibility could be negative and is usually so small in magnitude (of the order of 10^{-5} S.I.) that the associated anomalies are not observable in aeromagnetic data. One exception is halite, where large volumes accumulated in salt domes can have subtle negative anomalies in an otherwise subdued aeromagnetic background (Isles and Rankin, 2013). *Paramagnetic* minerals have the induced field in the same direction as the applied field, so the susceptibility is positive. Examples of paramagnetic mineral are amphiboles, pyroxenes and micas. The impact of these minerals is also subtle in aeromagnetic data (Isles and Rankin, 2013), although the magnitude of the susceptibilities of these minerals are about a factor of 100 greater than the diamagnetic minerals, being of the order of $1x10^{-3}$ S.I. or less. *Ferromagnetic* minerals, or more specifically ferrimagnetic minerals, such as the iron-titanium minerals like magnetite and maghemite, have much larger induced fields and susceptibilities of the order of $1000x10^{-3}$ S.I. These values are for the pure and massive samples of these minerals; however, these iron-titanium minerals are typically not a dominant fraction of the rock, so the susceptibilities of the rocks containing a few percent of these minerals are typically between $1x10^{-3}$ and $100x10^{-3}$ S.I.

When a rock containing ferromagnetic minerals has a static magnetic field that exists when there is no applied field, then this magnetic field, **R**, is called the remanent magnetic field. This field can be in any direction and is called a remanent field as it has been created by a process the rock experienced during sedimentation, metamorphism, alteration, or whilst being intruded. The strength of the remanent field is measured relative to the induced field and is given by the Koenigsberger ratio, Q, where (Dentith and Mudge, 2014)

$$Q = \frac{|\mathbf{R}|}{|\mathbf{M}|}. \qquad (3)$$

The Koenigsberger ratio can be measured using standard paleomagnetic laboratory instrumentation (e.g. Enkin, 2012) or a more portable instrument recently introduced by Schmidt and Lackie (2014).

If a magnetic survey is conducted to better understand the local geology, magnetic susceptibility is one physical quantity which can be used to link lithology and mineralogy to the survey response. Byrne et al. (2018) show how a magnetic susceptibility study can be an effective exploration tool for deposit-scale studies. They measured the outcrop magnetic susceptibility at the Highland Valley Copper Mine in British Columbia, and found that fresh (least altered) rocks have values corresponding to a geometric mean greater than $50x10^{-3}$ S.I.; a mixture of fresh and altered rocks corresponds to a range between ~$15x10^{-3}$ to $50x10^{-3}$ S.I.; and altered rocks and leucocratic dikes correspond to less than ~$15x10^{-3}$ S.I.. At the Canadian Malartic gold deposit, low magnetic susceptibility values correlate with an increase in gold concentration (Bérubé et al., 2018; Bérubé et al., 2019). These examples are quite localized and small scale. In general, the magnetic susceptibility is not a useful tool in more regional studies for characterizing rock types. This is because the range of values of the magnetic susceptibility for many rock types overlap with each other, and the value is more indicative of magnetite content than the rock type (Clark and Emerson, 1991).

A common use of magnetic susceptibility measurements is to characterize a lithology's magnetic properties to compliment forward modelling or data inversion. As magnetic susceptibility varies in different terrains, it is not always possible to use tabulated values (e.g. Clark and Emerson, 1991) for specifying a susceptibility of a particular rock type. One way of addressing this issue is

to collect a suite of susceptibility values in each terrain that is to be modelled. The validity of this approach will be assessed in this study.

1.4 Structure of the remainder of the thesis

The next chapter (Chapter 2) will introduce the data, software, and methodology being used in this thesis. This chapter will also discuss some theory and information for the data transformation processes used in this study. After this, the results will be presented (Chapter 3) and discussed (Chapter 4). Finally, Chapter 5 will provide a conclusion for this investigation.

CHAPTER 2

2 Methodology

2.1 Outline

In this chapter, I introduce the magnetic susceptibility data, the aeromagnetic data used in the study and the process for transforming this to the apparent susceptibility.

2.2 Data Types

2.2.1 Magnetic Susceptibility Data

The magnetic susceptibility data is sourced from the OGS Miscellaneous Data release 273—Revised (Muir, 2012). This dataset contains 28985 magnetic susceptibility data points across geologically prospective areas around the province. These data were collected using two different models of magnetic susceptibility meters: the KT-9 and KT-10 models. Table 1 lists each device's specifications. The most notable differences between the two devices is that the

KT-10 is sensitive to susceptibilities an order of magnitude smaller than the KT-9 and a factor of 2 greater, up to $2000x10^{-3}$ S.I. (Terraplus Inc., 2017; Terraplus Inc., 1997).

Table 1 Specifications of the KT-9 and KT-10 magnetic susceptibility meters.

	KT-9	KT-10
Sensitivity [S.I.]	$0.01x10^{-3}$	$0.001x10^{-3}$
Measuring Ranges [S.I.]	$0.01x10^{-3}$ to $999x10^{-3}$	$0.001x10^{-3}$ to $1999.99x10^{-3}$
Operating Frequency [kHz]	10	10
Coil Sensor Diameter [mm]	65	65

Of the 28 985 samples in the data release, 7626 data points are taken on outcrops within the study area (Muir, 2012). For each location, 10 measurements were generally taken at a variety of positions around the outcrop. If there are one or more units apparent in the outcrop, then 10 measurements are taken on each unit. Multiple measurements are required to collect a statistical representation of the magnetic susceptibility of each unit. From these multiple readings, statistical parameters such as the average and median of the magnetic susceptibility for each outcrop lithology or lithologies are determined.

Both KT susceptibility meters measure the susceptibility by placing the sensor coil of the device against a flat sample surface. The reading will be more indicative of the primary lithology if the surface is not weathered, so the instrument operator is instructed to look for an unweathered surface. However, this is not always possible or easy, so generally, what looks to be a less weathered surface is selected for the measurement. Finding ten unweathered and flat surfaces surface is also not easy, and when a curved or angular surface is selected, the rock will be more distant from the sensor and the reading will be an underestimate of the actual susceptibility.

The meters sense the magnetic susceptibility by measuring the frequency of the current in the circuit. However, the frequency measurements drift depending on the ambient temperature and other instrument factors, so the procedure involves first measuring the frequency in air away from the sample (air is assumed to have zero susceptibility), then measuring the frequency on the sample and finally measuring the frequency in air again. The two readings in air are interpolated and this reading is compared with that of the sample to estimate the magnetic susceptibility (Terraplus Inc., 2017). The estimate can be inaccurate if the drift is not linear between the two air readings, or if the interpolation procedure is incorrect. Errors can also result if the air reading is not taken distant from susceptible or metallic material. Other inaccuracies can result when there is a geological hammer or other metallic objects close to the sample location. When the magnetic susceptibility of the sample is anisotropic (different in one direction than another), then the readings can vary significantly, for example if the coil is parallel or perpendicular to foliation (Hrouda, 1982; Dentith and Mudge, 2014). Further errors might occur is the wrong units are being used, or the values are incorrectly transcribed, stored, transferred or processed.

Within the study area, 63% of the average of the outcrop magnetic susceptibility measurements lie below $1x10^{-3}$ S.I.. Thirty-five percent of the values lie between $1x10^{-3}$ and $100x10^{-3}$ S.I.; only 162 data points (2%) have a value larger than $100x10^{-3}$ with only one value larger than $1000x10^{-3}$ S.I.. This distribution in the data is reflected throughout the whole MRD273 dataset as there are only 432 measurements greater than $100x10^{-3}$ S.I. out of the 28985 measurements the OGS has collected. These outcrops with a relatively high magnetic susceptibility likely contain magnetic minerals, such as magnetite or pyrrhotite. Figure 2 illustrates the locations of the outcrops with magnetic susceptibility data location (red circles) within the study area overlaying the geology data from Figure 1.

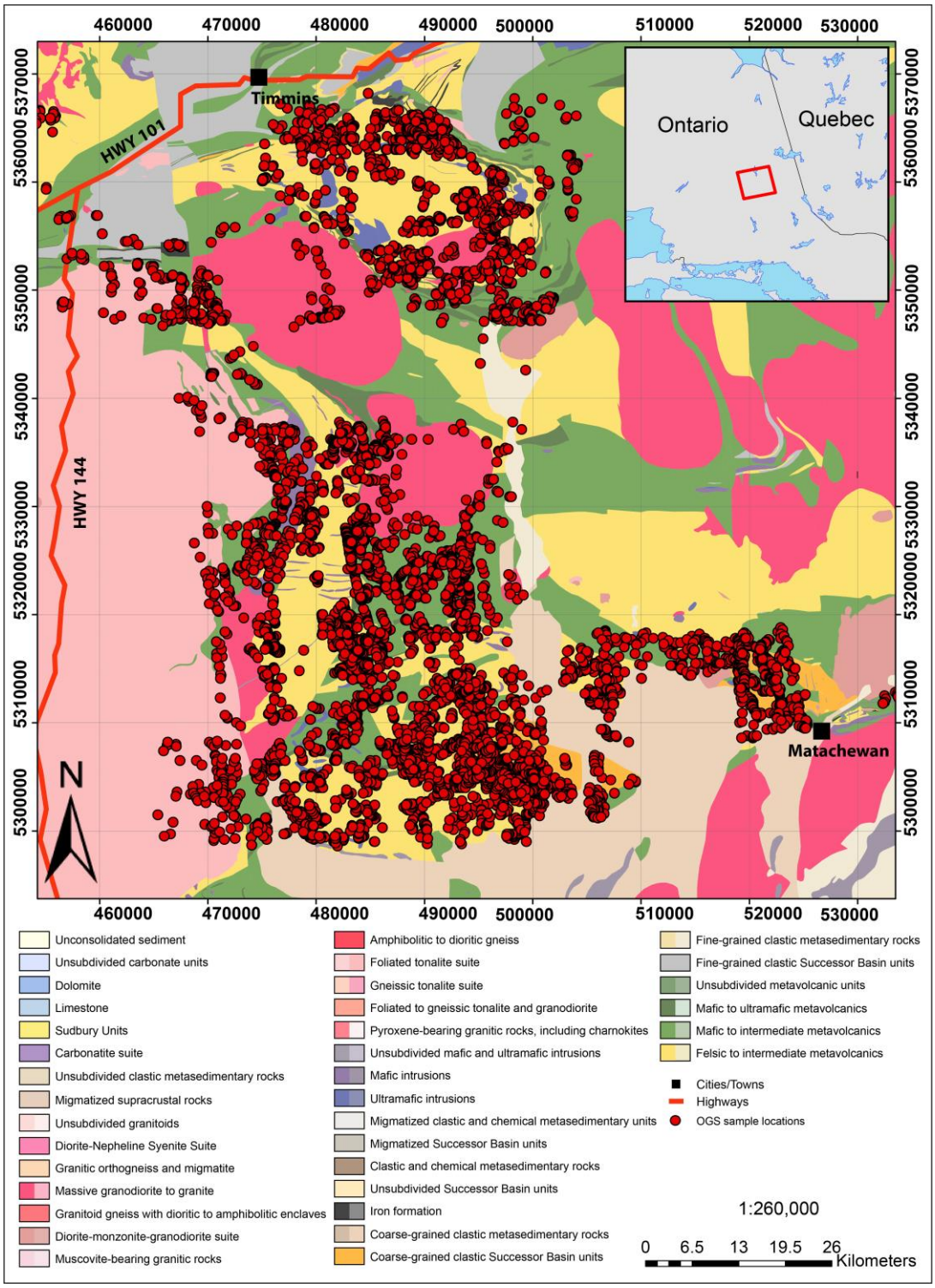

Figure 2 A map of the MRD273 outcrop magnetic susceptibility data, overlain on the geological map (Muir, 2012; OGS, 2011). Each red dot represents an outcrop where ten magnetic susceptibility readings were measured using a KT-9 or KT-10 susceptibility meter.

2.2.2 Airborne Magnetic data

The aeromagnetic grid shown in Figure 3 is part of the OGS Abitibi supergrid (OGS, 2017a) which is compiled from 20 different airborne magnetic surveys that have been converted to the same coordinate system (NAD83, UTM zone 17N), levelled, and stitched together (OGS, 2017b). Three of the 20 surveys had a trend removed before they were stitched, including the Round Lake Batholith dataset (OGS, 2017b), which covers the southeastern corner of the study area. More details on the specific techniques applied to each magnetic grid to incorporate them into the Abitibi supergrid can be found in OGS (2017b). The final compiled grid has been levelled to 70 m above the ground with a cell-size of 40 m. Within the study area, there are many small surveys with an average flight line spacing of 50 m, however a majority of the area was covered by surveys with an average traverse line spacing of 150 m or 200 m. This relatively high-resolution magnetic grid allows user to locate geological features with a high level of certainty. Nevertheless, we expect some disagreement when comparing the different sets of magnetic susceptibilities as the hand-held magnetic susceptibility measurements are valid for a very short distance from the measured locations (with a radius of centimeters) while aeromagnetic data are sensing the susceptibility in a volume that has a scale length more comparable to the sensor height.

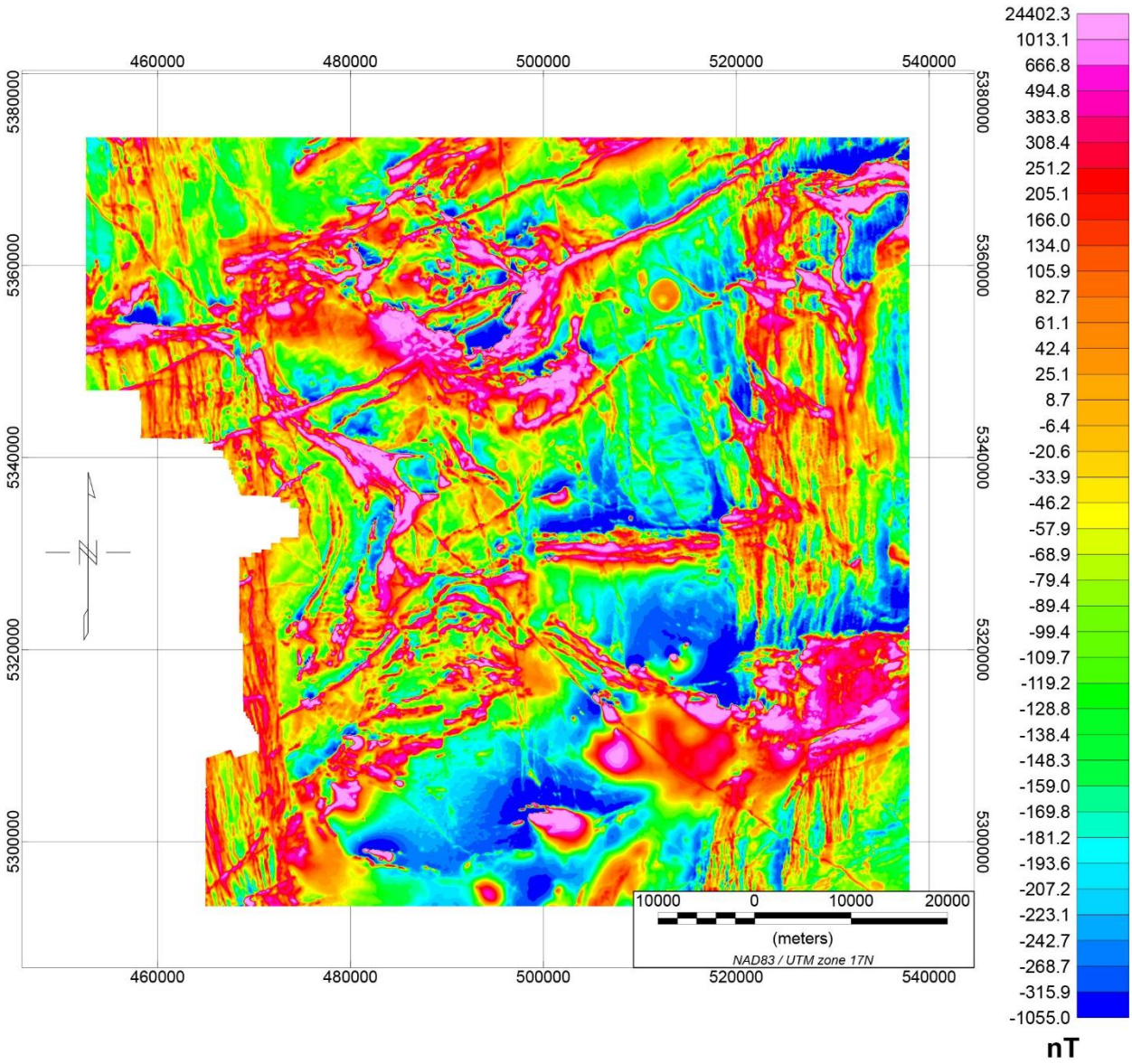

Figure 3 Total magnetic intensity grid data for the study location (OGS, 2017a).

2.3 Deriving Apparent Magnetic Susceptibility

Deriving an apparent magnetic susceptibility from TMI aeromagnetic data requires several steps, depending on the amount of processing which has already been applied. Generally, the first step is removing the geomagnetic field using the International Geomagnetic Reference Field (IGRF) at

the epoch the data was collected (Cain et al., 1967). This step has already been applied to the aeromagnetic data from the OGS. Next, there are three steps: first, reduce the data to the magnetic pole; secondly, apply a downward continuation on the data to the surface of the source; lastly, convert the induced magnetic field to an apparent magnetic susceptibility. In Geosoft's Oasis Montaj, this can be applied quickly using the apparent magnetic susceptibility tool within the "magmap" menu. In this tool, data are first converted to the two-dimensional wavenumber-domain using the fast Fourier transformation method. The reduction to pole and downward continuation are then linear operations (or filters) which can be applied directly to the wavenumber-domain data. The methodology of these operations will be discussed below.

2.3.1 Reduction to the Magnetic Pole

Due to the dipolar nature of the magnetic field, the shape and magnitude of a magnetic anomaly can vary depending on the orientation and direction of the inducing Earth's field and any remanent magnetization, which can be in an arbitrary direction. This can make it complicated to relate a measured field to its source. The reduction to the magnetic pole (RTP) process allows an interpreter to transform magnetic data from different latitudes to the data that would be measured if the Earth's field was vertical (as it is at the poles). This process simplifies the interpretation of the data; as magnetic highs at the poles generally occur over the centre of magnetic bodies. For example, in the study location south of Timmins, Ontario, the inclination and declination are approximately 74 and -11 degrees respectively and the TMI response of any magnetic anomalies will show as a magnetic high to the south and a small magnetic low to the north of the source. An RTP reduction was applied to the TMI grid in Figure 3 to derive Figure 4. Due to the filter centering the stronger positive part of the magnetic response directly above the source material,

the RTP grid has a closer correspondence to the magnetism of the rocks below than the TMI grid.

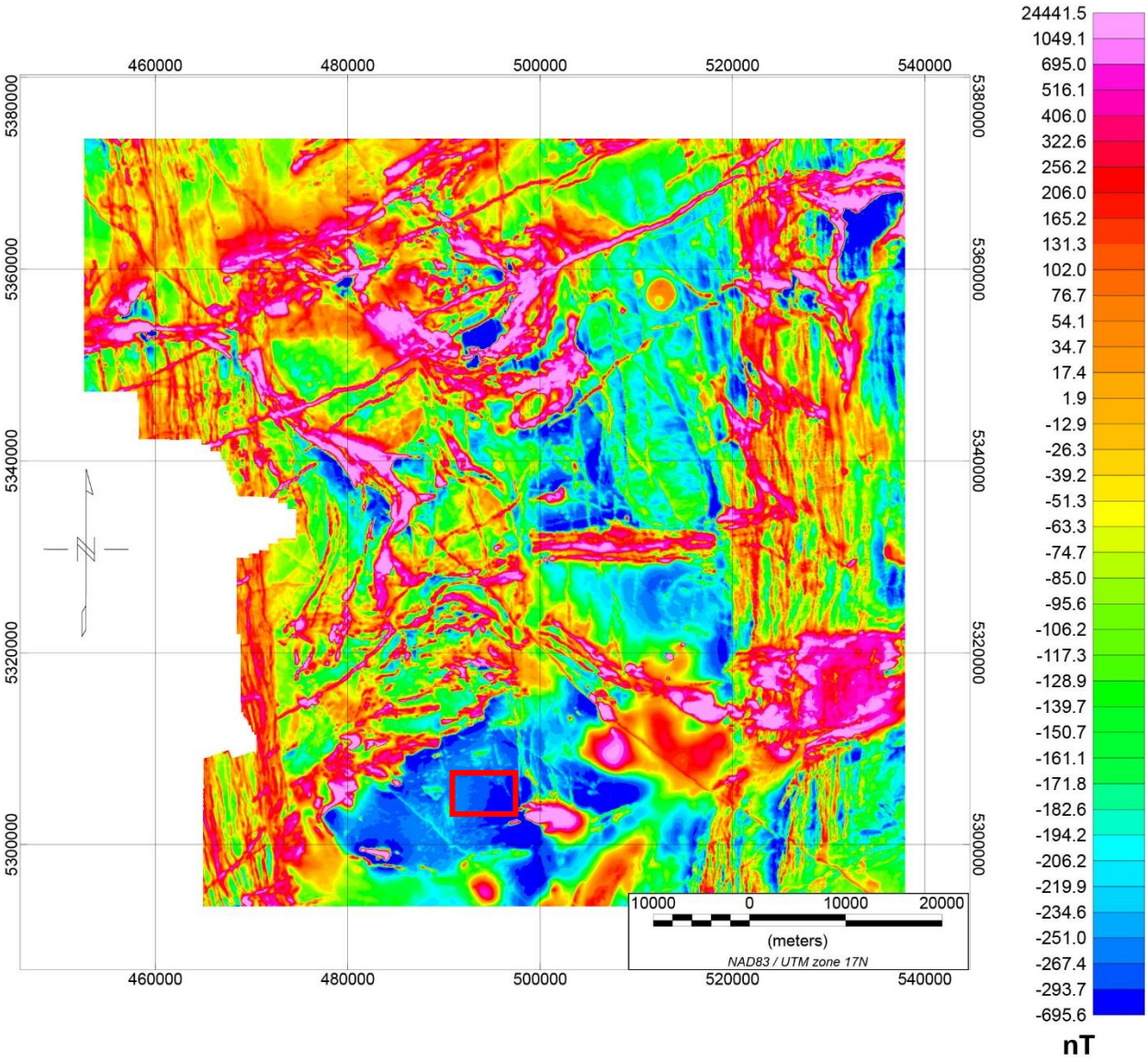

Figure 4 Aeromagnetic grid data after a reduction to the magnetic pole was applied to the total magnetic intensity grid data. Compared to Figure 3, anomalies in this grid will now lie directly above their corresponding sources, as long as there is no remanent magnetism present. The red box indicates an area used to correct the apparent magnetic susceptibility grid (Figure 5), described in the Appendix in Section 7.2.

An important assumption made when applying an RTP transformation to the data is that the magnetism of all rocks in the area is parallel to the geomagnetic field and due to induction only. Essentially this is assuming that remanent magnetization is small. Baranov and Naudy (1964) and Stewart (2019) describe RTP transformation, and more details on the calculations used in Oasis Montaj can be found in the help module of the software (Geosoft Inc., 2018c). At high magnetic latitudes, such as Timmins, the anomaly shapes are not shifted a significant distance, so the shifts are difficult to see at the scale that the data is shown. The lows (blue) to the north of each anomaly should have become less marked and a comparable amount of blue should appear to the south. The fact that this is not always seen implies that there is some remanent magnetization in the rocks.

2.3.2 Downward Continuation

A continuation filter is meant to transform the data from the original measurement height datum, to a datum which would have been measured at a different height above the source. An upward continuation increases the height above the source, while a downward continuation is an estimation of the field closer to the source. This method also relies on applying a filter to the Fourier transform of the data (Fuller, 1967). More details about the specific algorithm used can be found in Geosoft Inc. (2018b).

Continuation modifies the amplitude of the wavenumber spectrum. For downward continuation, short wavelengths are amplified and long wavelengths are suppressed, which in effect enhances the near-surface response. However, performing a downward continuation is unstable when the downward continuation distance is too large. The extent of instability will depend on the distance of continuation and the quality of the dataset. Most aeromagnetic noise is low amplitude (about 0.1 nT) and is at the sensor height. When this is downward continued, it will be amplified, the

amplification depends on the amplitude of the noise and the nature of the surrounding signal. When deriving apparent magnetic susceptibility, it is common practice to first apply a downward continuation to the data to the ground surface, which will correspond to the top of the shallowest possible magnetic sources. If this step is not applied, the apparent susceptibility estimate will be too small (Bambrick, 1982). However, due to the instability that can be introduced by applying too large a downward continuation, an experiment was conducted to understand when signal enhancement was large enough without noise enhancement being too large. Details of this experiment are described in the Appendix in section 7.1, where I concluded that a downward continuation distance of 70 m was appropriate.

In order to test the robustness of the downward continuation used in the magmap module of the Oasis Montaj software, the aeromagnetic grid (Figure 3) was downward continued 70 m and then the resulting grid was upward continued 70 m to the original height. Then, the difference between the resulting grid and the original grid were computed. The resulting grid showed small differences between the two, the largest value being 2.44×10^{-5} nT, a negligible amount.

2.3.3 Apparent Magnetic Susceptibility

Apparent magnetic susceptibility is derived using Equation (1). This equation describes the theory behind the apparent magnetic susceptibility (SUSC) tool used in Geosoft's Oasis Montaj software (Geosoft Inc., 2018a). This transformation can also be thought of as a crude inversion, a method to transform a measured field to a physical property. The input of this inversion would be the aeromagnetic grid data (**M**) and the IGRF field (**H**), and the susceptibility is given by Equation (1). The result is the spatial distribution of the magnetic susceptibility that is consistent with or would produce the measured data. Two assumptions are made when using this method: 1) all

magnetic response is a result of induction only, or no magnetic remanence is present, and 2) the Earth's surface is a collection of vertical rectangular prisms of grid-interval dimensions with their tops at the same height, infinite depth and a constant magnetic susceptibility. If these assumptions are not satisfied, the resulting apparent susceptibility anomalies will be distorted. The output is a grid with cell values that indicate the average apparent magnetic susceptibility for each 40 m by 40 m area (Figure 5). The apparent magnetic susceptibility filter produces a result in CGS units and had to be transformed to S.I. unit using Equation 2 for comparison with observed susceptibility values.

Geometrically, the grid in Figure 5 looks similar to the TMI grid, except some flight line and grid stitching artifacts have been emphasized by the downward continuation filter (as discussed in the downward continuation experiment in the Appendix in Section 7.1). In addition, the amount of short wavelength features has increased due to this enhancement process.

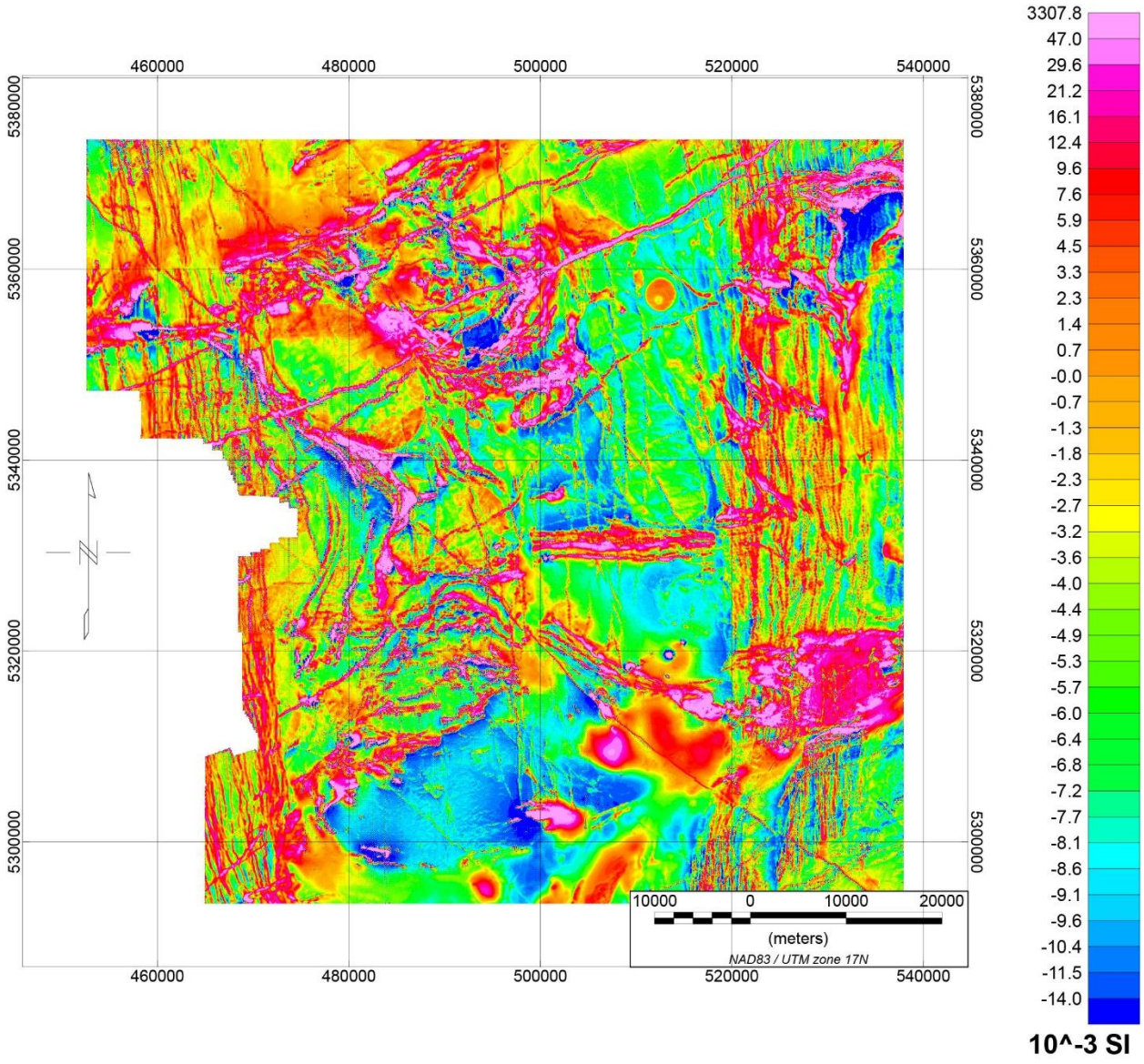

Figure 5 Apparent magnetic susceptibility after a downward continuation of 70 m to the surface of the terrain.

On Figure 5, as shown on the colour legend bar, note that all values represented with colors cooler than orange are negative. As a final step, the addition of an arbitrary magnetic susceptibility shift factor is recommended by Bambrick et al. (1982). This step is to correct for the regional field that is initially removed from the airborne magnetic data, which will affect the average apparent magnetic susceptibility for the survey area. The intention is to remove strong negative values as

they are unrealistic in areas where the magnetic susceptibility is expected to be close to zero. A number of large areas of relatively uniform negative values are visible in Figure 5, for example inside the red box in Figure 4. If the regional magnetic field had been removed correctly, small negatives would be adjacent to large positives as part of a dipole anomaly. This step is crucial, because without the correction 52% of the cells located where outcrop magnetic susceptibility exists (and is measured to be positive) have negative apparent susceptibilities. The process to determine a magnetic susceptibility correction factor is to first identify areas in the TMI grid where there are no anomalies and the magnetic susceptibility has been measured from outcrop samples and found to have low magnetic susceptibility. Areas like this should not produce a positive or negative anomaly on the apparent magnetic susceptibility grid. The next step is to calculate the average negative apparent magnetic susceptibility value in this area derived from the TMI value (**M**) and the IGRF value (**H**) using Equation 1. This apparent susceptibility value can now be added to the apparent magnetic susceptibility grid, to bring the apparent susceptibility in this area to a value consistent with those measured in the area, as is desired. Figure 6 shows the results of applying a positive shift of 10.335×10^{-3} S.I. to the grid in Figure 5, which removes many negative apparent magnetic susceptibility values and achieves a general agreement between calculated and measured properties in the area outlined in red on Figure 4. More details on this correction value can be found in the Appendix in Section 7.2. There still remain areas of the grid in Figure 6 that contain cells with negative apparent susceptibility. Due to this, 11% (828 outcrop measurements) cannot be compared with these negative apparent susceptibility values as few rock forming minerals exist with such large negative magnetic susceptibilities. This leaves 6695 outcrop locations where a comparison can still be made.

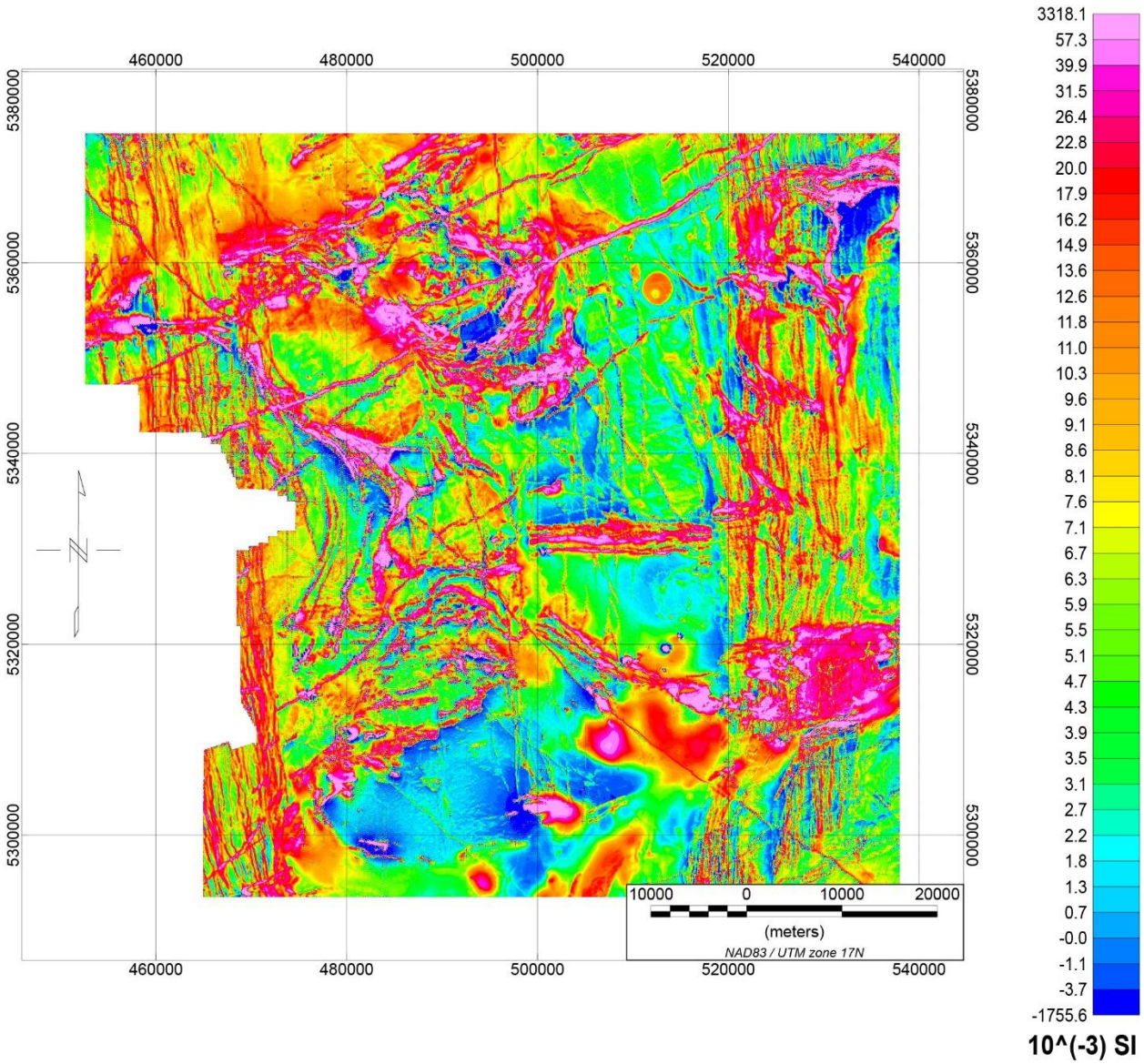

Figure 6 Apparent magnetic susceptibility with a DC shift correction for the TMI regional trend removal. Note that the DC shift correction applied to this grid did not fully eradicate negative apparent magnetic susceptibilities; it corrected the vast majority of the grid.

2.4 Comparing Outcrop Magnetic Susceptibility to Apparent Magnetic Susceptibility

In order to compare the OGS outcrop susceptibility readings with the apparent magnetic susceptibility grid, the grid will be sampled at every outcrop location (Figure 2) for which there is

a corresponding measured magnetic susceptibility value. The sampled grid value and the measured value at the same location are compared on a log-log plot (Figure 7). Due to a large range of magnetic susceptibility values a log-log plot can be more representative compared to a simple linear plot. Ideally, and if all assumptions are true, the two estimates should agree and the points will lie along a straight line with the unit slope.

2.5 Modelling Aeromagnetic Data

Two 2D models are created in order to test the usefulness of the outcrop magnetic susceptibility data when using it to model the aeromagnetic data. These are created using the GM-SYS 2D profile creator in Oasis Montaj. The location of the profile to be modelled is shown in Figure 1 as a blue line. The location was chosen to limit the geological complexity but maximize the outcrop magnetic susceptibility data located nearby. The profile is 30 km in length and generally perpendicular to strike, as GM-SYS assumes.

Creating a geological model which fits the geophysical data can be a challenging task, as it requires that the model be consistent with the known geological and geophysical information. Since the goal of this thesis is to investigate the usefulness of outcrop scale magnetic susceptibility, several initial assumptions will be made in order to simplify the task: i) all geological contacts are vertical; ii) each geological unit has a constant magnetic susceptibility; and iii) there is no magnetic remanence present. This final assumption is necessary as we have no remanence information. All three assumptions are analogous to the assumptions made in deriving the apparent magnetic susceptibility values.

The first model can be considered a starting point, or *a priori* model. To create this model, the lithological type and boundaries were taken from the OGS 2011 geological bedrock map and

combined with an average outcrop magnetic susceptibility as determined from outcrop measurements within the area covered by that lithology. This model is then refined to better fit the aeromagnetic data, producing the second model. In Figure 1, the profile location intersects 5 separate lithological units with three major rock types including felsic to intermediate metavolcaincs, mafic to intermediate metavolcanics, and granodiorite to granitic rock types (OGS, 2011). By comparing the response created by this *a priori* model to the data, an initial idea of the usefulness of using the mapped geology and the mean of the outcrop measurements can be gained.

Chapter 3

3 Results

3.1 Apparent Magnetic Susceptibility Comparison

The measured outcrop magnetic susceptibility readings range in value between 0 and $1020x10^{-3}$ S.I. and the apparent magnetic susceptibility values ranged between $0.0018x10^{-3}$ and $505x10^{-3}$ S.I., but Figure 7 has been restricted to show values between $1x10^{-5}$ and $1000x10^{-3}$ on each axis because a majority of the values lie in this range.

Two groups are present on Figure 7. Group 1 contains outcrops with average magnetic susceptibility readings less than $1x10^{-3}$ S.I.. This group has a trend that follows a horizontal line. Group 2 contains outcrop magnetic susceptibility readings between $1x10^{-3}$ and $200x10^{-3}$ S.I.. This group plots within one order of magnitude of the red 1:1 correlation line. Of the 6695 outcrops that are included in the final comparison between the two data types, 4056 exist in Group 1 (~60% of the measurements) and 2639 exist in Group 2 (~40% of the measurements). Each rock type displays the same two populations, with varying degrees of clarity.

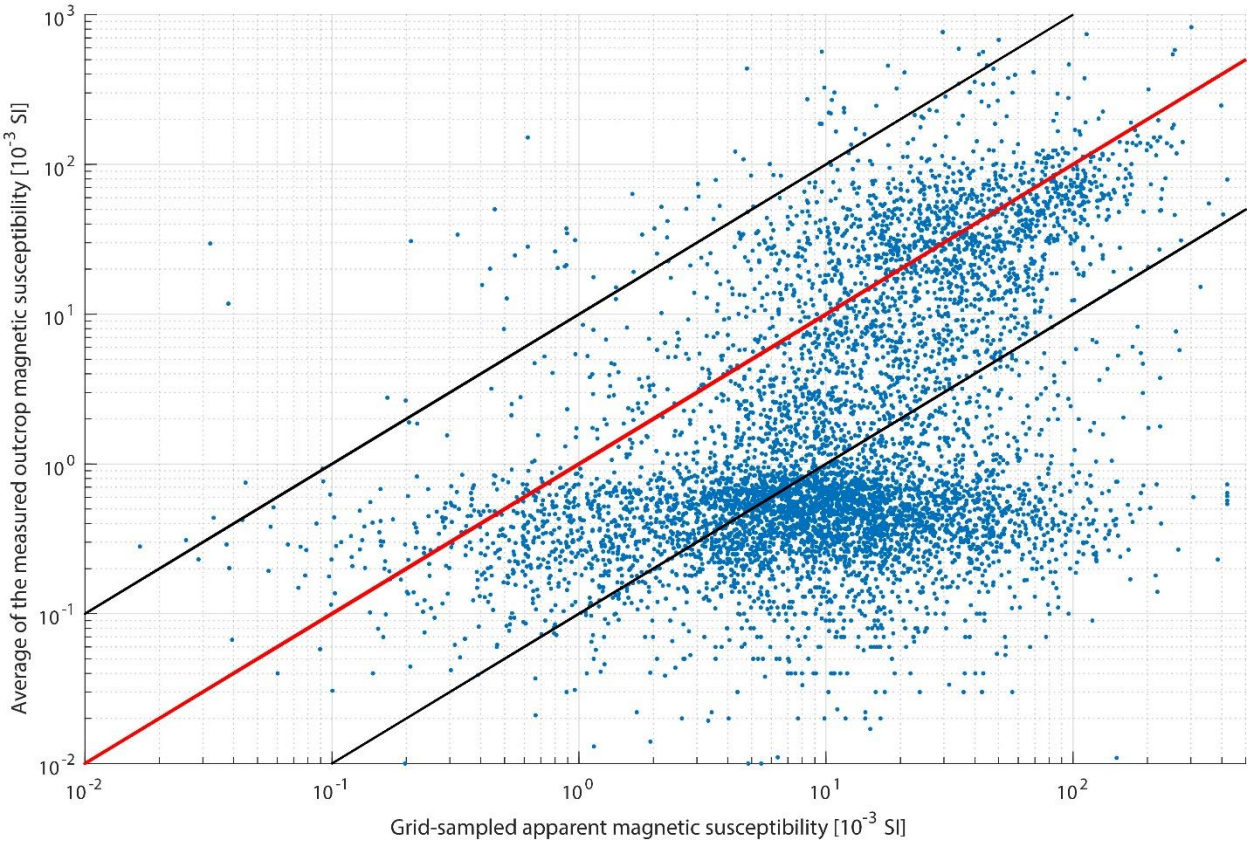

Figure 7 A log-log plot with the average calculated magnetic susceptibility on the x-axis and the average outcrop magnetic susceptibility on the y-axis. Units for both axes are presented in 1x10^{-3} S.I.. The red line indicates a hypothetical equality line between the two data sets and the black lines indicated an envelope whereby points lying outside of these lines have an apparent magnetic susceptibility value that differs from the measured value by at least one order of magnitude.

3.2 2D Modelling of Aeromagnetic Data

Figure 8 illustrates the *a priori* model introduced above. Each of the five lithologies intersected on the profile have a corresponding area on the geological map. The outcrop magnetic susceptibilities within each of these areas were averaged to give a mean value for that lithological area. These lithologies have been labelled L1 though L5 with the following outcrop-measurement mean

magnetic susceptibility values: L1 has a susceptibility of $0.5x10^{-3}$ SI, L2 has a susceptibility of $11.4x10^{-3}$ SI, L3 has a susceptibility of $1.5x10^{-3}$ SI, L4 has a susceptibility of $11.6x10^{-3}$ SI, and L5 has a susceptibility of $13x10^{-3}$ SI.

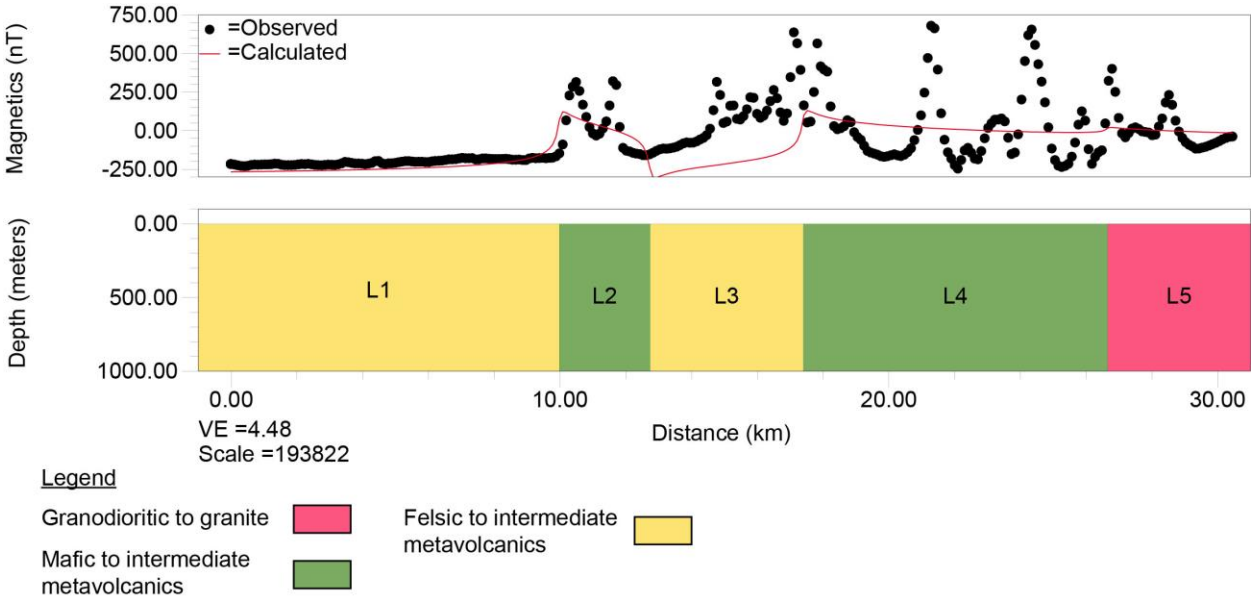

Figure 8 Priori model combining the geological and means from magnetic susceptibility databases. The location of this profile is shown in Figure 1 by the blue line. The three different rock types are felsic to intermediate metavolcanics (yellow), mafic to intermediate metavolcanics (green), and granodiorite and granite (pink). (Source of initial data: OGS, 2011; Muir, 2012)

The response of the *a priori* model shown in Figure 8 fits the observed data poorly. In the south, a less magnetic lithology (L1) is fit well by the average magnetic susceptibility approximation. As well in the north, L5's observed magnetism is reasonably approximated, except for a magnetic anomaly in the center of the granodioritic body. The observed magnetism of L2, L3, and L4 are not fit well by this model. This seems to be due to a more complex geology than what the bedrock map indicates. Since average values were used for each lithology, it is reasonable that the calculated magnetic field is between the peaks and valleys of the observed data. The data indicates that within each of the five sections there are some sub-units that are more magnetic and some which might be less magnetic.

Figure 9 illustrates the refined model where the calculated model response was fit to the observed model response by inserting sub-lithologies into each major lithology and allowing the magnetic susceptibility values to vary by up to an order of magnitude. On Figure 9, the colours representing a rock type were assigned so as to represent a range of magnetic susceptibility values. In the case of the mafic to intermediate metavolcanic lithologies, I define 2 ranges (light green corresponding to a susceptibility between value $5x10^{-3}$ SI to $15x10^{-3}$ SI, and dark green corresponding to a susceptibility value between $15x10^{-3}$ SI and $42x10^{-3}$ SI). All changes to the interpreted magnetic susceptibility of each sub-unit is within one order of magnitude, consistent with Figure 7.

Additionally, two new lithologies were interpreted; a diabase dyke in the north (black) and a blue unit corresponding to mafic to ultramafic rocks (Figure 9). The dyke is interpreted from a linear magnetic feature clearly evident on the aeromagnetic map but not shown on the geology map. The mafic to ultramafic lithology is interpreted to exist because the geological feature on the OGS (2011) bedrock map, which lies adjacent to the profile has a magnetic anomaly that can be seen extending into the profile on the aeromagnetic map. In order to determine an appropriate starting point for the susceptibility of the diabase and mafic/ultramafic units, outcrop susceptibility measurements associated with corresponding rock types in nearby locations were averaged. The maximum error between the calculated and observed magnetic response in Figure 9 is 38 nT.

In the refined model (Figure 9), L1 was not changed in any way from Figure 8 because the fit was sufficiently close. In order to fit the magnetic anomalies, L2 was divided into 5 different sub-lithologies; three light green units corresponding to a lower range of values and two dark green units correspond to a higher range. L3 is less magnetically homogeneous when compared to L1, so L3 was subdivided into several magnetic mafic to intermediate metavolcanic units and two mafic to ultramafic sub-lithologies in order to explain the magnetic anomalies. Some of these sub-

lithologies were thin; the thinnest having an apparent thickness of 150 m. The original felsic to intermediate sub-lithologies within the L3 section have magnetic susceptibility values between $0.5x10^{-3}$ SI and $10x10^{-3}$ SI. Unit L4 was split into many sub-lithologies in order to explain the large and small magnetic anomalies throughout the lithology. The calculated magnetic responses within L5 compare well with the measured data. Fortuitously, it was not necessary to change the susceptibility of the major lithology (grandodioritic/granitic rock) from the average value estimated from the near outcrop samples ($13x10^{-3}$ SI). The diabase dyke interpreted within L5 fit the measured data with a magnetic susceptibility value of $27.5x10^{-3}$ SI.

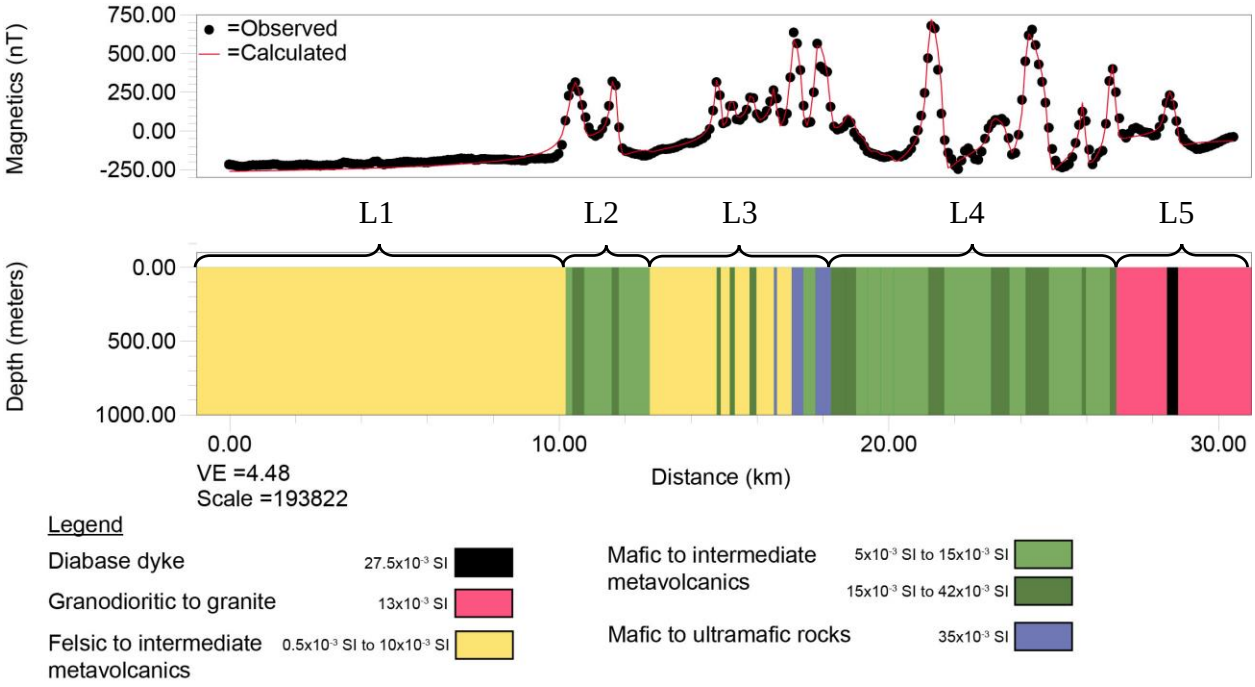

Figure 9 The interpreted magnetic model. This model was created by using Figure 8 as a starting point and introducing sub-lithologies with varying the magnetic susceptibilities in order to fit the observed aeromagnetic data. Two new rock types are included: mafic to ultramafic rocks and a diabase dyke. Any changes made to magnetic susceptibility were smaller than 1 order of magnitude difference from the average outcrop magnetic susceptibility value for each rock type. The bracket labels indicate where the original 5 lithologies from the bedrock map existed. (source of initial data: OGS, 2011; Muir, 2012)

Chapter 4

4 Discussion

The apparent magnetic susceptibility calculation has a varying degree of success at approximating the magnetic susceptibilities of outcrops. There is a weak correlation seen in Group 2 (green ellipse on Figure 10) which indicates that the apparent susceptibility calculation somewhat resolves the magnetic susceptibility of outcrops within this range ($1x10^{-3}$ to $200x10^{-3}$ S.I.). Of the 2639 outcrops in Group 2, 2320 (87.9%) data points lie within 1 order of magnitude of the red line in Figure 7. The scatter of Group 2 does not sharpen towards the red line as the magnetic susceptibility of the outcrop increases. In fact, for outcrops with a magnetic susceptibility measured higher than $100x10^{-3}$ S.I., there is no evident trend in the data, and data is sparse. Furthermore, there is a distinct lack of data on outcrops with magnetic susceptibility greater than $100x10^{-3}$ S.I.. Values greater than $100x10^{-3}$ S.I. are anomalous and only occurs within anomalously magnetic minerals and it is unlikely to measure this range at a regional scale.

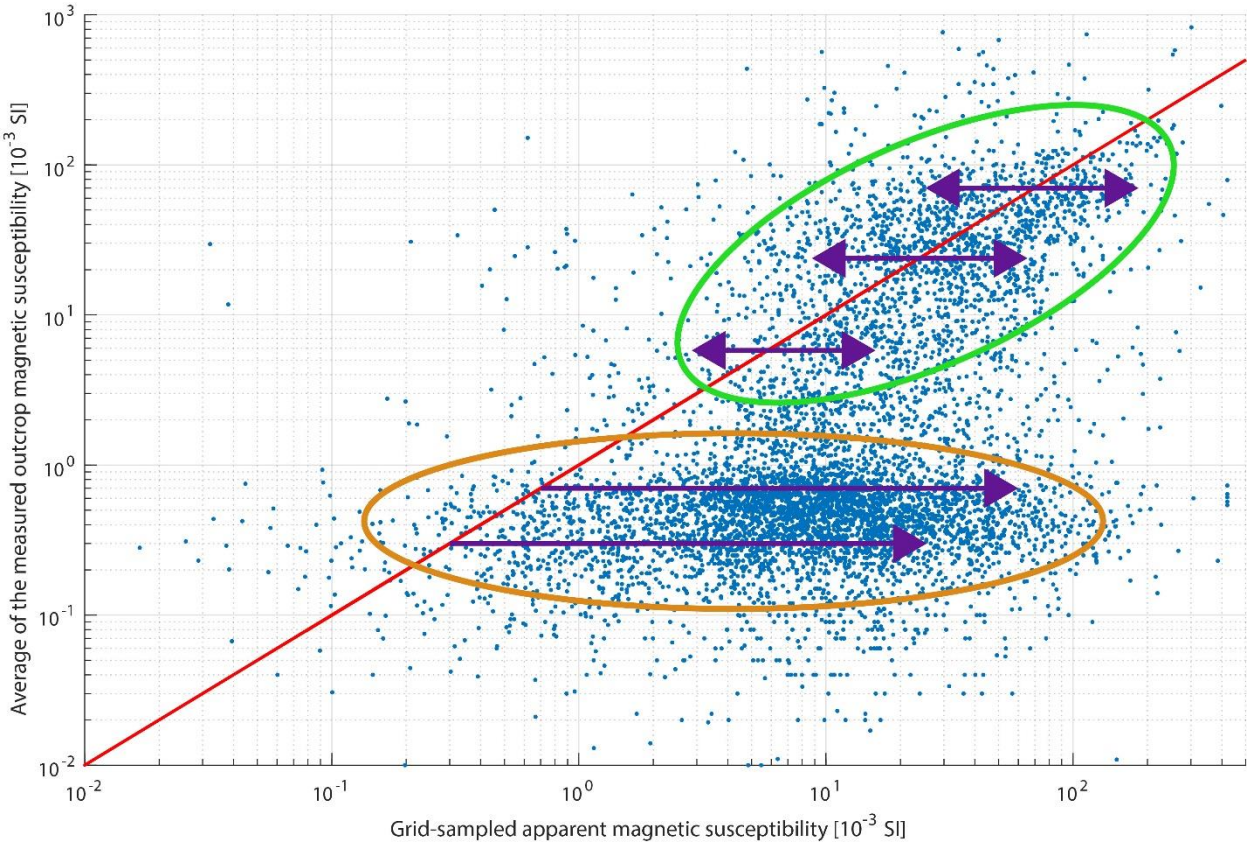

Figure 10 A log-log plot with the average calculated magnetic susceptibility on the x-axis and the average outcrop magnetic susceptibility on the y-axis. Units for both axes are presented in 1x10^{-3} S.I.. The red line indicates a hypothetical equality line between the two data sets. Group 1 (population circled in orange) apparent magnetic susceptibility data does not correlate with the average outcrop magnetic susceptibility, while Group 2 (population circled in green) weakly correlates. The purple arrows indicate shifts from the red line which symbolize the factors that affect the comparison, discussed in Chapter 4.

The lack of correlation seen in Group 1 (orange ellipse on Figure 10) indicates that the apparent susceptibility calculation poorly resolves the magnetic properties of rocks with a low magnetic susceptibility measurement (less than 1x10^{-3} S.I.). The overall poor estimation provided by the apparent susceptibility calculation is likely due to a combination of several factors. These factors include the different sampling, coverage, and resolution regimes of the two datasets, the

assumptions that are made when calculating the apparent magnetic susceptibility, magnetic remanence, anisotropy, and potential errors within the magnetic susceptibility dataset, all of which will be discussed in more detail below.

The first reason is that the aeromagnetic data was collected at a different scale than the outcrop magnetic susceptibility data. This is often the case when comparing a dataset collected using airborne methods versus ground-based method. The apparent magnetic susceptibility derived using the apparent magnetic susceptibility filter is the average value for the 40 m by 40 m cell (OGS, 2017a). In contrast, the outcrop susceptibility data points are an average of 10 individual measurements, each sensitive to an area of about 6 cm, which is much smaller than the grid cell size. These susceptibility measurements can only be taken where there is not overburden, resulting in limited and spotty coverage. Furthermore, the magnetic susceptibility meters only sense magnetism from rocks immediately in front of the sensor, while an airborne magnetometer senses magnetism from a much larger volume of rock, to potentially much greater depth, thus the ground based measurements will often be an underestimate of the airborne apparent susceptibility measurements. The rocks in group 1, with smaller measured susceptibilities, will be more easily overwhelmed by the magnetic field of nearby or deeper magnetic features. This additional field explains the overestimate of the apparent magnetic susceptibility and the spread of group 1 to the right.

A second reason is that there may be a violation of the assumption that the earth is made up of multiple square prisms with the same magnetic susceptibility from a flat surface to infinite depth (magnetically homogeneous). If the susceptibility suddenly decreases below the surface, then the effect of what is near the surface will be spread to all depths, meaning that the apparent susceptibility will underestimate what is measured near surface. Conversely, when the measured

susceptibility is low at surface, but if there is a sudden increase in susceptibility at depth, then the apparent susceptibility will be more than what is measured at surface. This is related to the first reason above, in that magnetic bodies below (or to the side) are having an impact. This provides another explanation for the stronger spread seen in group 1.

The third reason for poor correlation is that the susceptibility is unlikely to be homogeneous over a 40 by 40 m cell. Daigneault et al. (2002; 2004) have recorded the tectonic history of the Abitibi subprovince and reported two major deformation zones, both which run through the study area. Thus, the structural complexity of the study area indicates the assumption that each source prism would have a constant magnetic susceptibility is not realistic. Geological features, such as folds and faults (and terrain), create a non-homogeneous and complex volume and are also pathways for meteoric (or magmatic) fluids which can disrupt the homogeneity of rock susceptibility through weathering (or alteration), and further affect the results of the apparent susceptibility calculation. To a lesser extent, overburden such as soils and glacial till can add further uncertainty to the homogeneity of each source prism. These geometry factors are compounded by the varying terrain over the study area. The ground is not composed of the vertical semi-infinite prisms with a flat top surface which the apparent susceptibility filter assumes. Hence it is not a surprise that one or two outcrops in an area could not always have identical susceptibilities to all the rocks in the prism.

Fourthly, the reduction to the pole transformation assumes that there is no remanent magnetization present in the rock. If remanent magnetization is present, the overall magnetism of the rock will be a sum of the induced magnetism (Equation 1) and the remanent magnetization. Depending on the orientation and magnitude of the remanence, this would result in an over or underestimation of the induced magnetization, and consequently either over or underestimated calculated magnetic susceptibility. As briefly mentioned in section 2.3.1, an indication of the presence of remanent

magnetization can be seen when the results of a reduction to the magnetic pole do not collapse dipolar anomalies to a monopolar anomalies, or do not remove strong negatives to the north. The nature of the negatives evident on the map can be used to infer that there is some remanence in the rocks, however, it is not easy to estimate the strength or orientation of this remanence from the magnetic data. Within the data used to make this comparison, there are 171 susceptibility measurements taken on diabase dyke material. A Majority of these dykes are Proterozoic and have a remanent magnetism. However, roughly 75% lie within population 1. This is likely an unreliable observation, and can be explained by the KT-10 measurements underestimating the magnetic susceptibility of the material as a result of surface weathering.

Irving and Naldrett (1977) performed a paleomagnetism study, or natural remanent magnetism (NRM) study, in the Abitibi subprovince. They determined the NRM of three units (the Kamiskotia complex, the Dundonald sill, and an unspecified group of Archean gabbro and lavas) and the NRM of several sets of Matachewan and Abitibi diabase dikes. Multiple areas were studied, including locations in the centre and western parts of this paper's study area, and north of this paper's study area. They concluded that the presence of NRM is found to be complex, as demagnetization occurred at an 80 m margin on either side of the diabase dikes intruding through remanent units (Irving and Naldrett, 1977). In order to understand and quantify NRM of all units over all the study area would require significantly more paleomagnetic measurements.

Fifthly, while the individual aeromagnetic data sets were all levelled to be at a height of 70 m above terrain, this will not be a flat horizontal surface due to variations in terrain. The downward continuation process assumes a horizontal surface, so this erroneous assumption will result in some distortions and a lack of correlation on Figure 7.

Sixthly, if there is anisotropy in the magnetic susceptibility, then this could explain some scatter in the measured values, depending on the orientation of the surface used to measure the susceptibility. Anisotropy could also scatter the measured aeromagnetic values depending on the orientation of the anisotropy with respect to the orientation of the earth inducing magnetic field.

There might also be some errors, including transcription errors, operation errors, or poor procedures, in the magnetic susceptibility measurements. For example, the KT-9 and KT-10 devices have options to record in S.I. or CGS units, the selection of which does not get recorded with the final measurement. Additionally, there is a protocol with the OGS to avoid weathered surfaces and to use flat surfaces where the coil sensor can be held flush (Muir, 2012). However, it is not easy to find the perfect measurement locations on each outcrop. Rather than finding an unweathered surface an operator might find a nearby less weathered surface, or the flattest surface in easy reach. As well, the conductivity of certain minerals, such as magnetite can cause a slight over-estimation of the susceptibility (Clark and Emerson, 1991).

The arrows on Figure 10 is one attempt to explain how the points may have moved away from the red line representing equality. For the large magnetic susceptibilities (group 2), the material will be ferromagnetic and are more likely to have a remanent magnetization. If this remanence is in the same direction as the induced field, it will increase the apparent magnetic susceptibility estimate (right arrow), but it is in the opposite direction, it will decrease the estimate (left arrow). There appears to be a comparable amount of increase and decrease, suggesting that the remanence is as likely to be in the same direction as the opposite direction. If a more accurate estimate of the magnetic properties of the outcrop sample is required for modelling, it would be necessary to measure the magnetic remanence as well as the magnetic susceptibility. An accessible instrument

for measuring the susceptibility and remanence has recently become available (Schmidt and Lackie, 2014; Schmidt, 2015).

The points in the less magnetic group (1) are most likely to be paramagnetic or felsic (Enkin et al., 2012) and not likely to be remanently magnetized. However, if they have a strong magnetic body nearby or below, then once the magnetic anomaly associated with this body has been reduced to the pole, its anomaly will primarily be positive. This positive anomaly will add to the magnetic field and increase the apparent magnetic susceptibility. Hence the arrows in group 1 are to the right and can result in a shift as large as the most magnetic material in the survey area as these materials must be nearby some non magnetic outcrop locations.

The aeromagnetic data is derived from multiple surveys collected at different times, it is important to understand the change of the field over time. Using the IGRF tool in Oasis Montaj, Figures 16 and 17 (Appendix Section 7.3) were created to illustrate the change in the IGRF between the year that the aeromagnetic data in the supergrid were collected from (1975) to the published year (2017). As seen in Figure 16, the total magnetic intensity of the Earth's magnetic field has been declining over the years. Additionally, the inclination and declination have been changing as well (Figure 17). The reduction to the pole and the apparent magnetic susceptibility calculations both require a single value for the total field strength. This could cause further error to be introduced during the calculation of apparent magnetic susceptibility. Furthermore, if the inclination and declination aren't precise the maps geometry and amplitudes could be negatively affected. This factor could have further affected the poor correlations in the comparison.

Whether the rock is paramagnetic or ferromagnetic material, will have a strong control over the susceptibility value (Enkin et al. 2020). This is highly dependant on the mineralogy (primarily

ferromagnesium silicates and magnetite) and the geochemistry of the sample. Thus, including mineralogical and geochemical information with the magnetic susceptibility database could see an increase in accuracy. Specifically, lab or portable X-ray transmission (XRT) information could provide a quick measurement method to determine iron content.

In order to produce the model response in Figure 9, sub-lithologies were interpreted along the profile. However, since magnetic susceptibility is only indicative of iron mineral content (Clark and Emerson, 1991), these sub-lithologies cannot be considered new or separate geological lithologies, they should be considered as different sub-lithologies. These sub-lithologies could indicate that there can be multiple sources of magma with different iron content within a volcanic package. Or they might represent alteration or metamorphism of the rock.

Chapter 5

5 Conclusion

This study has found that there is not a strong correlation between the magnetic susceptibility as measured on outcrop samples and those inferred from aeromagnetic data. Outcrops with a measured average magnetic susceptibility that is weak (below $1x10^{-3}$ S.I.) do not show any correlation at all with aeromagnetic data, likely because the magnetic field of a nearby or underlying body is interfering and has increased the apparent susceptibility estimate. However, the outcrops with a measured average susceptibility above $1x10^{-3}$ S.I. show a weak to moderate correlation with the estimates from the aeromagnetic data, generally agreeing within a factor of ten. This result is acceptable considering the wide range of magnetic susceptibilities and the large uncertainties associated with very local measurements of magnetic properties. Our modelling suggests that the variation is most likely due to local heterogeneities in magnetic susceptibility

and/or remanent magnetization. Variabilities in the susceptibility by a factor of ten or more is consistent with statistical studies on large numbers of samples (Eshaghi et al., 2019)

Hence, when modelling data, the modeller can use a magnetic susceptibility measurement made on an outcrop as a rough estimate in their model, when the value is more than $1x10^{-3}$ S.I. However, the modeller has the flexibility to adjust this rough estimate by a factor of ten in order to explain the measured data. If tighter constraints are required for modelling or inversion, there are a number of strategies. One is measuring the magnetic remanence and susceptibility, but since the remanence measurement requires extra effort, we suggest that this is only undertaken when the susceptibility of the rock that is measured is greater than $1x10^{-3}$ S.I. The other strategy is to measure the heterogeneity of the susceptibility on surrounding or similar rocks. This will give the modeller an indication of more or less magnetic material that might be nearby or underneath the sample location that may be causing a magnetic anomaly.

When the measured outcrop value is less than 10^{-3} S.I., the resulting magnetic anomaly is small, so more magnetic material below or to the side of the measured value is even more likely to have an impact. These small measured values are also likely to be impacted by other sources of error (operator error, instrument noise, anisotropy, inhomogeneity, etc).

Despite the lack of correlation found between the apparent and outcrop magnetic susceptibilities, using a mean value of the outcrop magnetic susceptibility in order to form an *a priori* model when modelling or inverting aeromagnetic data appears helpful at the start. Particularly in cases where the rock in questions is magnetically homogenous and/or non-magnetic. However, due to the heterogeneous nature of magnetic susceptibility and bimodal distribution of susceptibility data, the statistical distribution of the values in a large database can be used to justify varying the

susceptibility in order to fit magnetic anomalies. As such, these outcrop magnetic susceptibility measurements, when statistically analysed, are useful as a guide to range of values that can be used for modelling aeromagnetic data.

Chapter 6

6 References

Bambrick, J., Letros, S., Strangway, D. W., and Geissman, J., 1982, Apparent magnetic susceptibility (SUSC) mapping in theory and practice: SEG Technical Program Expanded Abstracts 1982, 238-241.

Bérubé, C. L., Olivo, G. R., Choteau, M, Perrouty, S., Shamsipour, P., Enkin, R. J., Morris, W. A., and Thiémonge, R., 2018, Predicting rock type and detecting hydrothermal alteration using machine learning and petrophysical properties of the Canadian Malartic ore and host rocks, Pontiac Subprovince, Québec, Canada: Ore Geology, **96**, 130-145.

Bérubé, C. L., Olivo, G. R., Choteau, M, and Perrouty, S., 2019, Mineralogical and textural controls on spectral induced polarization signatures of the Canadian Malartic gold deposit: Applications to mineral exploration: Geophysics, **84**, B135-B151.

Cain, J. C., Hendricks, S. J., Langel, R. A., and Hudson, W. V., 1967, A Proposed Model for the International Geomagnetic Reference Field-1965*: Journal of Geomagnetism and Geoelectricity, **19**, 335-355. DOI: https://doi.org/10.5636/jgg.19.335

Clark, D., 1997, Magnetic petrophysics and magnetic petrology; aids to geological interpretation of magnetic surveys: AGSO Journal of Australian Geology and Geophysics, **17**, 83–103.

Clark, D. A. and Emerson, D. W., 1991, Notes on Rock Magnetization Characteristics in Applied Geophysical Studies: Exploration Geophysics, **22**, 547-555.

Daigeneault, R., Mueller, W. U., and Chown, E. H., 2002, Oblique Archean subduction: accretion and exhumation of an oceanic arc during dextral transpression, Southern Volcanic Zone, Abitibi Subprovince Canada: Precambrian Research, **115**, 261-290.

Daigeneault, R., Mueller, W. U., and Chown, E. H., 2004, Abitibi greenstone belt plate tectonics: the diachronous history of arc development, accretion and collision: Developments in Precambrian Geology, **12**, 88-103.

Deng, D. N., and Smith, R.S., 2016, A comparison of magnetic susceptibility meters using samples from the Thompson Nickel Belt, Canada: Preview, October, 41-44.

Enkin, R J., Cowan, D., Tigner, J., Severide, A., Gilmour, D., Tkachyk, A., Kilduff, M., Baker, J., 2012, Physical property measurements at the GSC paleomagnetism and petrophysics laboratory, including electric impedance spectrum methodology and analysis: Geological Survey of Canada, Open File 7227. https://doi.org/10.4095/291564

Enkin, R. J., 2014, The Rock Physical Property Database of British Columbia, and the distinct petrophysical signature of the Chilcotin basalts: Canadian Journal of Earth Sciences, **51**, 327–338. Doi: dx.doi.org/10.1139/cjes-2013-0159

Enkin, R. J., Hamilton, T. S., Morris, W. A., 2020, The Henkel petrophysical plot: mineralogy and lithology from physical properties. Geochemistry, Geophysics, Geosystems, **20**, https://doi.org/10.1029/2019GC008818.

Eshaghi, E., Smith, R. S., Ayer, J., 2019, Petrophysical characterisation (i.e. density and magnetic susceptibility) of major rock units within the Abitibi Greenstone Belt: Laurentian University Mineral Exploration Research Centre, publication number MERC-ME-2019-144.

Fuller, B.D., 1967, Two-dimensional frequency analysis and design of grid operators, in Hansen, D. A., Heinrichs, W. E., Holmer, R. C., MacDougall, R. E., Rogers, G. R., Sumner, J. S., Ward, S. H. (eds), Mining Geophyscs, Vol II, theory, Society of Exploration Geophysicists, pp 658-708. DOI: 10.1190/1.9781560802716.ch4

Gaucher, F. E. S. and Smith, R. S., 2017, The impact of magnetic viscosity on time-domain electromagnetic data from iron oxide minerals embedded in rocks at Opemiska, Québec, Canada: Geophysics, 82(5), B165-B176. https://doi.org/10.1190/geo2017-0153.1

Geosoft Inc, 2018a, Apparent Susceptibility Calculation (SUSC), https://my.geosoft.com/supportcentre#/help/oasismontaj-extensions-fft2con_susc.htm, accessed 20 June 2019.

Geosoft Inc, 2018b, Downward Continuation (CNDN), https://my.geosoft.com/supportcentre#/help/oasismontaj-extensions-fft2con_cndn.htm, accessed 20 June 2019.

Geosoft Inc, 2018c, Reduce to the Magnetic Pole (REDP), https://my.geosoft.com/supportcentre#/help/oasismontaj-extensions-fft2con_redp.htm, accessed 20 June 2019.

Halls, H.C., Stott, G.M. and Davis, D.W., 2005, Paleomagnetism, geochronology and geochemistry of several Proterozoic mafic dike swarms in northwestern Ontario: Ontario Geological Survey, Open File Report 6171, 59p.

Hrouda, F., 1982, Magnetic anisotropy of rocks and its application in geology and geophysics: Geophysical Surveys, **5**, 37–82.

Irving, E. and Naldrett, A. J., 1977, Paleomagnetism in Abitibi greenstone belt, and Abitibi and Matachewan diabase dikes: Evidence of the Archean geomagnetic field: The Journal of Geology, **85**, 157-176.

Isles, D. J., and Rankin, L. J., 2013, Geological Interpretation of aeromagnetic data. Australian Society of Exploration Geophysicists. www.aseg.org.au/publications/geological-interpretation-aeromagnetic-data. Accessed August 13, 2019.

Krogh, T. E., Corfu, F., Davis, D. W., Dunning, G. R., Heaman, L. M., Kamo, S. L., Machado, N., Greenough, J. D., and Nakamura, E., 1987, Precise U–Pb isotopic ages of diabase dykes and mafic to ultramafic rocks using trace amounts of baddeleyite and zircon: Mafic dyke swarms. Geological Association of Canada, Special Paper 34: 147-152.

Lelièvre P. G., Oldenburg, D. W., and Williams, N. C., 2009, Integrating geological and geophysical data through advanced constrained inversions: Exploration Geophysics, **40**, 334-341. https://doi.org/10.1071/EG09012

Mahmoodi, O., Smith, R., 2015, Clustering of downhole physical property measurements at the Victoria property, Sudbury for the purpose of extracting lithological information: Journal of Applied Geophysics, **118**, 145–154. doi.org/10.1016/j.jappgeo.2015.04.015

Mahmoodi, O., Smith, R. S. and Spicer, B., 2017, Using constrained inversion of gravity and magnetic field to produce a 3D litho-prediction model. Geophysical Prospecting, **65**, 1662–1679. doi:10.1111/1365-2478.12484

Mahmoodi, O., Smith, R. S. and Tinkham, D. K., 2016, Supervised classification of down-hole physical properties measurements using neural network to predict lithology: Journal of Applied Geophysics, **124**, 17-26. doi:10.1016/j.jappgeo.2015.11.006

Monecke, T., Mercier-Langevin, P., Dubé, B., and Frieman, B. M., 2017, Geology of the Abitibi Greenstone Belt, Reviews in Economic Geology, **19**, 7-49.

Muir, T. L. 2013, Ontario Precambrian bedrock magnetic susceptibility geodatabase for 2001 to 2012; Ontario Geological Survey, Miscellaneous Release—Data 273 – Revised.

OGS (Ontario Geological Survey), 2011, 1:250 000 scale bedrock geology of Ontario; Ontario Geological Survey, Miscellaneous Release–Data 126 - Revision 1, http://www.geologyontario.mndm.gov.on.ca/mndmaccess/mndm_dir.asp?type=pub&id=MRD126-REV1. Accessed 20 June, 2019.

OGS (Ontario Geological Survey), 2017a, Ontario airborne geophysical surveys, magnetic data, grid data (ASCII and Geosoft® formats), magnetic supergrids. Geophysical data set 1037 -- Revised (GDS1037), http://www.geologyontario.mndm.gov.on.ca/mndmaccess/mndm_dir.asp?type=pub&id=GDS1037-REV. Accessed June 13, 2019.

OGS (Ontario Geological Survey), 2017b, Ontario airborne geophysical surveys, magnetic supergrids: Geophysical data set 1037—Revised, http://www.geologyontario.mndm.gov.on.ca/mndmfiles/pub/data/imaging/GDS1037-REV//GDS1037-REV_report.pdf. Accessed June 13, 2019.

Schmidt, P. W., and Lackie, M. A., 2014, Practical considerations: making measurements of susceptibility, remanence and Q in the field: Exploration Geophysics, **45(4)**, 305-313. DOI: 10.1071/EG14019

Schmidt, P. W., 2015, The Qmeter - a portable tool for remanence and susceptibility: ASEG Extended Abstracts, 2015, **1**, 1-3. DOI: 10.1071/ASEG2015ab235

Smith, R., Shore, M, and Rainsford, D., 2012, How to make better use of physical properties in mineral exploration: The exploration site measurement: The Leading Edge, **31**, March, 936-940. https://doi.org/10.1190/1.3694901

Stewart, I. C. F., 2019, A simple approximation for low-latitude magnetic reduction-to-the-pole; Journal of Applied Geophysics, **166**, 57-67, accessed 20 June 2019; https://www.sciencedirect.com/science/article/pii/S0926985118310127?via%3Dihub

Terraplus Inc., 1997, User's Guide, KT-9 Kappameter, Rev. 1, 80p.

Terraplus Inc., 2017, User's Guide, KT-10 v2 Magnetic Susceptibility, Conductivity and Combined Magnetic Susceptibility / Conductivity Meter, 115p.

Thurston, P. C., Ayer, J. A., Goutier, J., and Hamilton, M. A., 2008, Depositional Gaps in Abitibi Greenstone Belt Stratigraphy: A Key to Exploration for Syngenetic Mineralization: Exonomic Geology, **103**, 1097-1134.

Chapter 7

7 Appendices

7.1 Downward Continuation Experiment

A downward continuation filter refers to a type of wavenumber filter in which short wavelengths are amplified and long wavelengths are suppressed, which in effect enhances the near-surface response. Mathematically, the filter input is a measurement on one (upper) measurement surface and the output is what would be measured on a lower measurement surface. While this filter can be advantageous when attempting to recover or enhance information about near-surface features in airborne magnetic surveys where these features might be attenuated at the upper surface, performing a downward continuation using too large of a distance between the upper and lower surfaces can lead to an unstable result. As such, if applied improperly, a downward continuation can result in amplification of noise and poorly characterized anomalies. Some factors which control the amplitude of the noise and limit the distance that the data can be downward continued are collection height, data resolution, and data quality. However, in most cases, the processing geophysicist can only control the distance of downward continuation, and decide (usually quantitatively) whether the continuation distance is too large. This appendix section will serve to document the experiments undertaken by the author to determine the appropriate downward continuation distance for the data of this study.

Three apparent magnetic susceptibility grids were produced: one with no downward continuation (collection height of 70 m above the surface) (Figure 11), another with a 70 m downward continuation applied ("collection height" 0 m above the surface) (Figure 13), and an intermediate grid halfway between these two cases with a 35 m downward continuation applied ("collection height" 35 m above the surface) (Figure 12). As this experiment's purpose is to assess the effectiveness of downward continuation procedures alone, no further corrections (such as used in Section 7.2) will be applied. On these three grids there are several features that highlight the instability of the downward continuation filter. In Figure 10 the downward continuation has introduced short wavelength artefacts in the grid that cause a misaligned or cross-hatched look in the data. These artefacts only run north-south and east-west (Figure 14 c), and are likely flight line artefacts emphasized by the downward continuation. These artefacts are visible to a lesser extent in the 35 m downward continuation "halfway" case (Figure 14 b), but not on the original grid (Figure 14 a).

To quantitatively understand how these instabilities in the downward continuation impacts the comparison between the measured susceptibility and calculated apparent susceptibility, the comparison has been made in each of the three cases. This was done by calculating the correlation coefficient between the measured outcrop magnetic susceptibility (in the interval from $1x10^{-3}$ to $1x10^{1}$ S.I.) and the calculated apparent susceptibility. A higher correlation value means that the two datasets correlate better. This interval is chosen for two reasons: 1. the magnetic susceptibility less than $1x10^{-3}$ S.I. contribute very little to the aeromagnetic signal, and 2. there is a moderate correlation between the two susceptibilities in the range above $1x10^{-3}$ S.I. Table 2 summarizes the results obtained in the three cases. The second column of the table lists the total number of useable (positive) samples at the comparison locations. The instability results in there being less of these

as the height gets lower. However, the greater downward continuation distance results in the amplitude of the anomalies increasing, so there are actually more useable (positive) values in group 2 above $1x10^{-3}$ S.I.. When these larger values are correlated, the correlation coefficient is actually larger. So although the greater continuation distance results in a noisier image, for our purposes, the results are better. Hence we have elected to continue the data down 70 m to the ground surface.

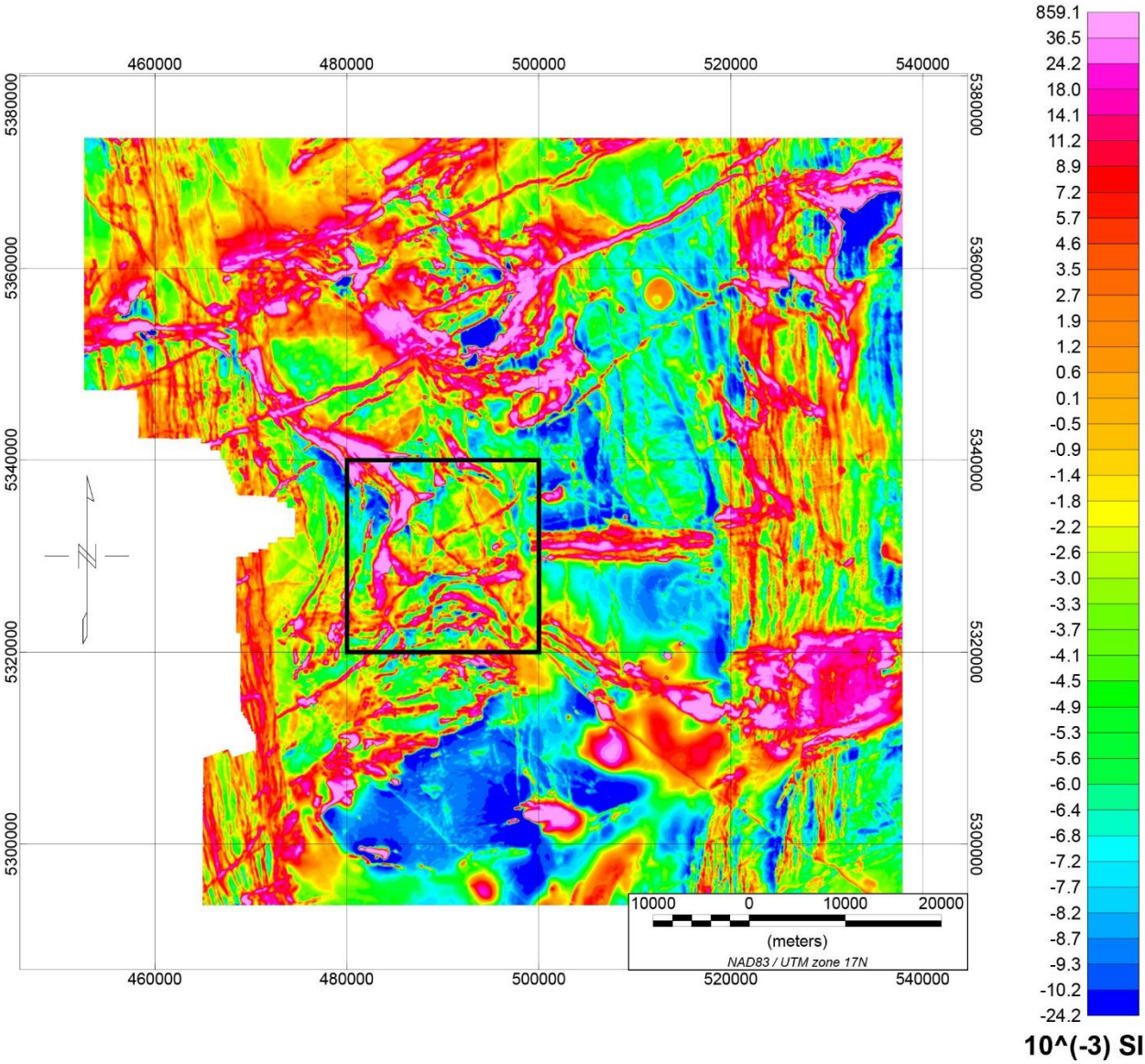

Figure 11 Apparent magnetic susceptibility grid with no downward continuation applied. The black box indicated the location of Figure 14 a.

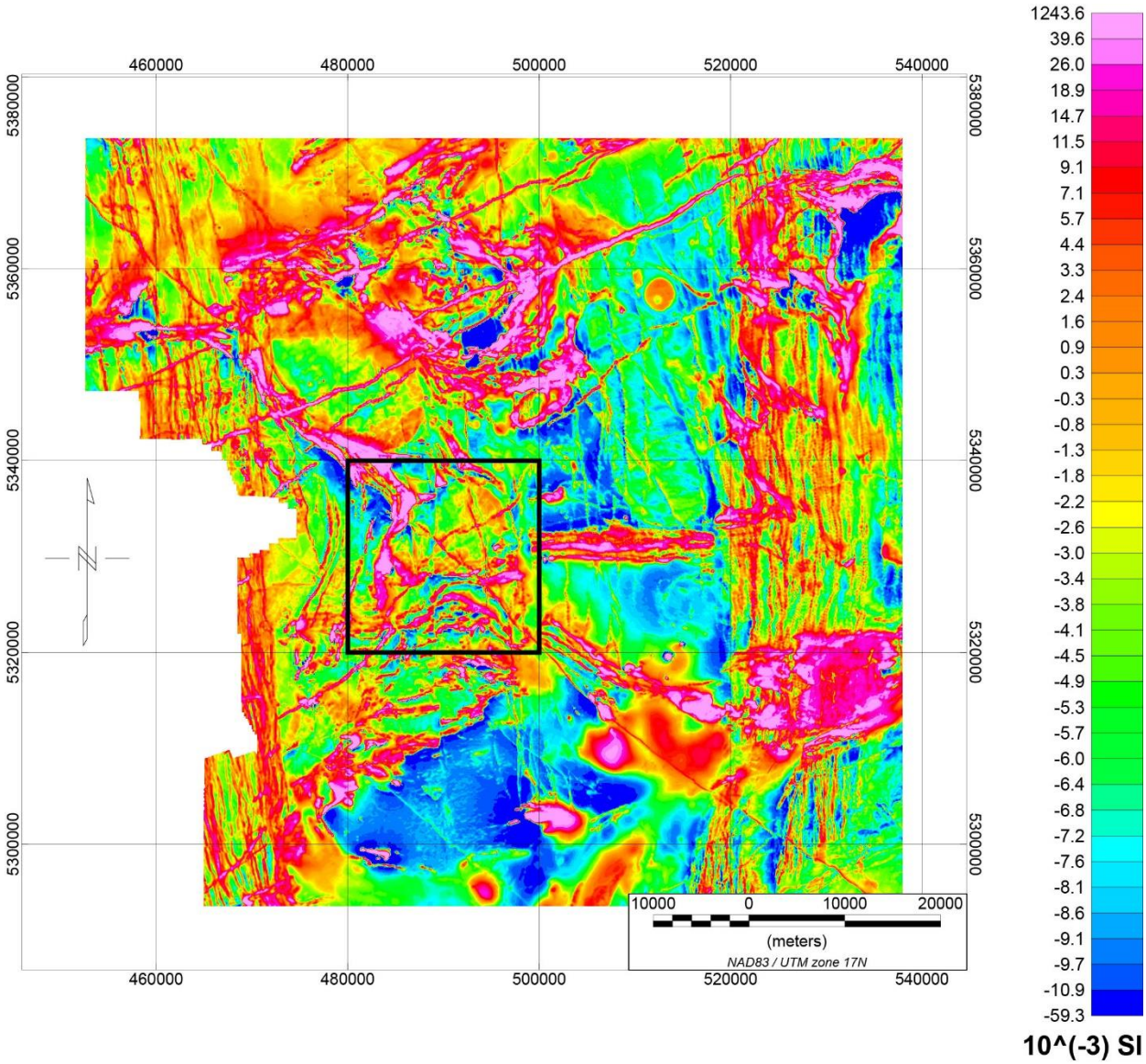

Figure 12 Apparent magnetic susceptibility grid with a downward continuation of 35 m applied (half way to source from collection height). The black box indicates the location of Figure 14 b.

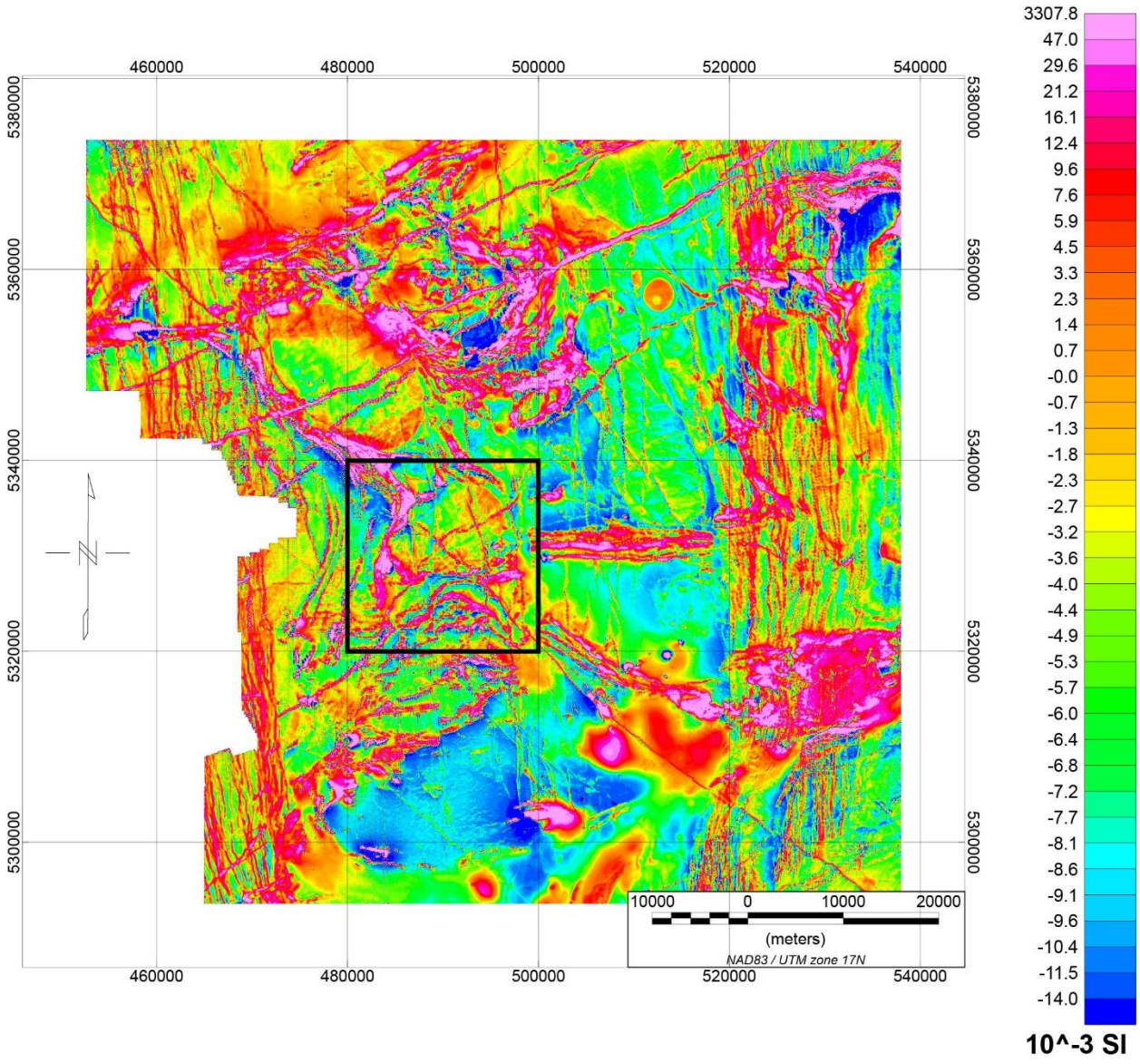

Figure 13 Apparent magnetic susceptibility grid with a downward continuation of 70 m to source height applied. The black box indicates the location of Figure 14 c.

Table 2 Summary of the parameters of interest for the downward continuation experiment. Each values were derived from the corresponding downward continuation height grid from this appendix.

Collection height after downward continuation (m)	Useable (positive) cell count after SUSC filter	Useable (positive) cell count greater than $1x10^{-3}$	Correlation coefficient
70 (Figure 11)	3965	1850	0.2665
35 (Figure 12)	3872	1866	0.2751
0 (Figure 13)	3622	1937	0.2813

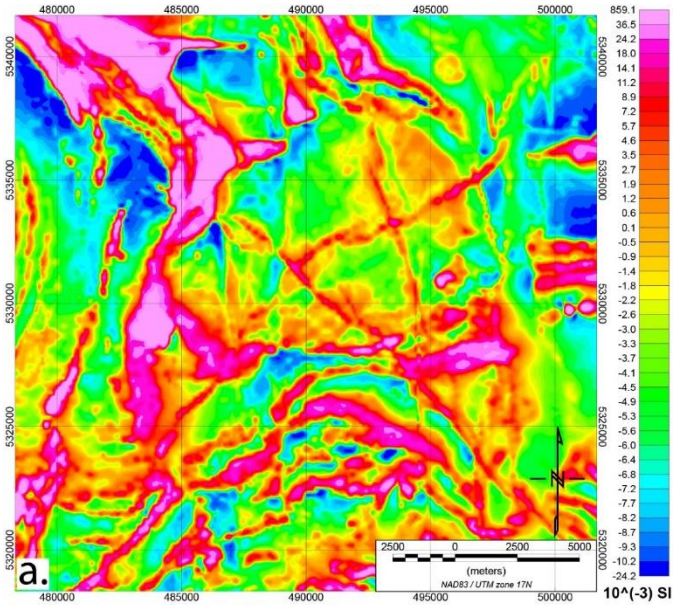

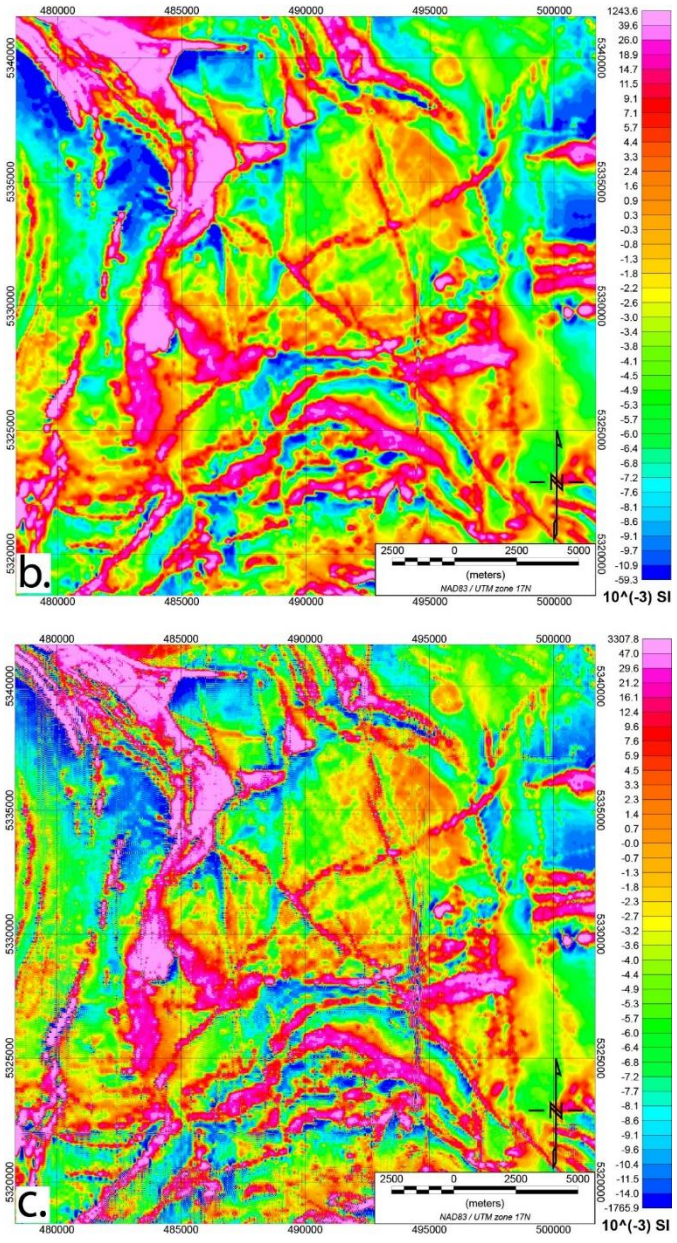

Figure 14 a. Zoomed in area sampled from Figure 11. b. Zoomed in area sampled from Figure 12. c. Zoomed in area sampled from Figure 13. By comparing Figures a., b., and c. the artefacts introduced during the downward continuation process can be identified.

7.2 Shift Correction of the Apparent Magnetic Susceptibility Grid

This appendix section describes how the arbitrary magnetic susceptibility shift is applied to the apparent magnetic susceptibility grid (Figure 5). Although the analysis in Section 7.1 has not had the shift correction applied, this step is still deemed crucial for the generation of figures 6 to 8 because 52% of the grid cell locations in Figure 5 where there is outcrop magnetic susceptibility have negative apparent susceptibility values. As previously described, the goal is to identify an area with material that is non-magnetic, both in the field measurements and in the TMI grid. The area used is outlined in Figure 4 by the red box. This area is composed of felsic to intermediate volcanics and coarse-grained successor basin units (Figure 1) (OGS, 2011), and shows no evidence of magnetic dikes intruding in the TMI grid (Figure 4). Within this area there are 225 outcrop magnetic susceptibility data points (Figure 15), with an average of 0.312×10^{-3} S.I.. There is no remanence information available, however, remanence is not likely as these values are typical of paramagnetic material (Enkin, 2014), which does not normally retain a remanent field. Also, the quantitative successful behaviour of the RTP filtering in this area suggest no evidence of significant remanence. The field is also relatively flat magnetically and there does not appear to be significant interference from nearby or underlying magnetic bodies.

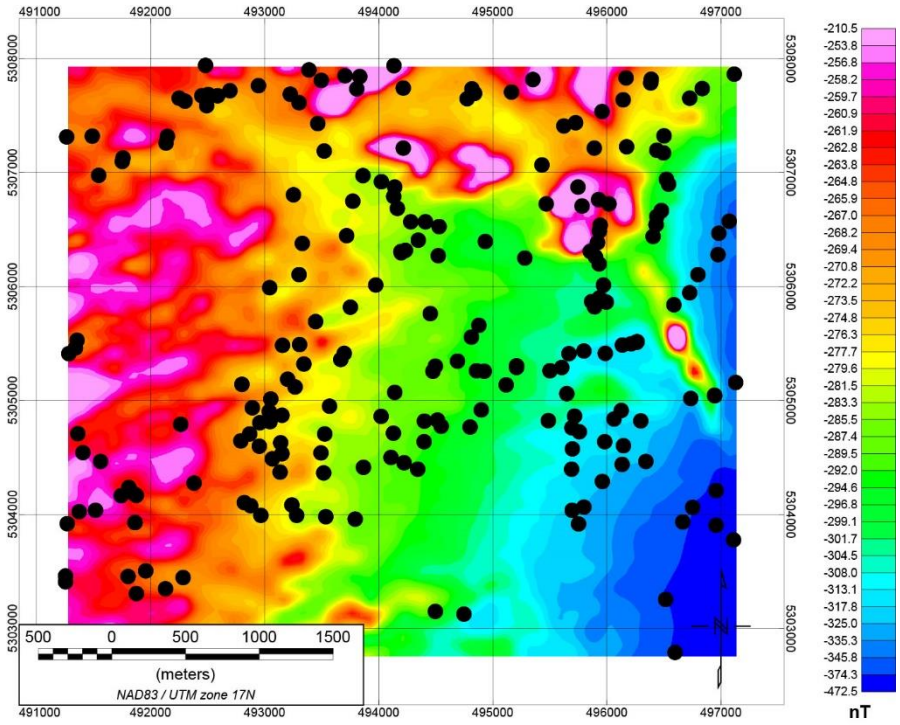

Figure 15 Reduced to the magnetic pole total magnetic intensity of the area outlined in red in Figure 4 that was chosen to correct for the regional trend removal (OGS, 2017a). The black points represent the 225 outcrops where the OGS collected magnetic susceptibility data (Muir, 2012).

Figure 15 displays the total magnetic intensity of the area (reduced to the magnetic pole), which varies by approximately 220 nT. The next step is to calculate the apparent magnetic susceptibility using the apparent magnetic susceptibility tool in Geosoft Inc.'s Oasis Montaj software. Averaging these gives an average apparent magnetic susceptibility for this area of -10.023×10^{-3} S.I., which is a large negative value generated by the IGRF removal. However, if we assume this area is essentially non-magnetic, then a value of 10.335×10^{-3} S.I. should be added to the apparent susceptibility grid, to give a much smaller and positive average apparent susceptibility value of 0.312×10^{-3} S.I. (which is the average of the measured values in the same area) and this is what has been done to generate Figure 6.

7.3 International Geomagnetic Reference Field Changes Over Time

The following plots show the magnitude of the magnetic field (Figure 16) and the inclination and declination (Figure 17), estimated from the IGRF formula over the period that magnetic data within the study area were collected. The magnitude varies by 6%, so there will be a corresponding change in the magnetic anomalies over the same period. The changes in inclination and declination are less than 10%.

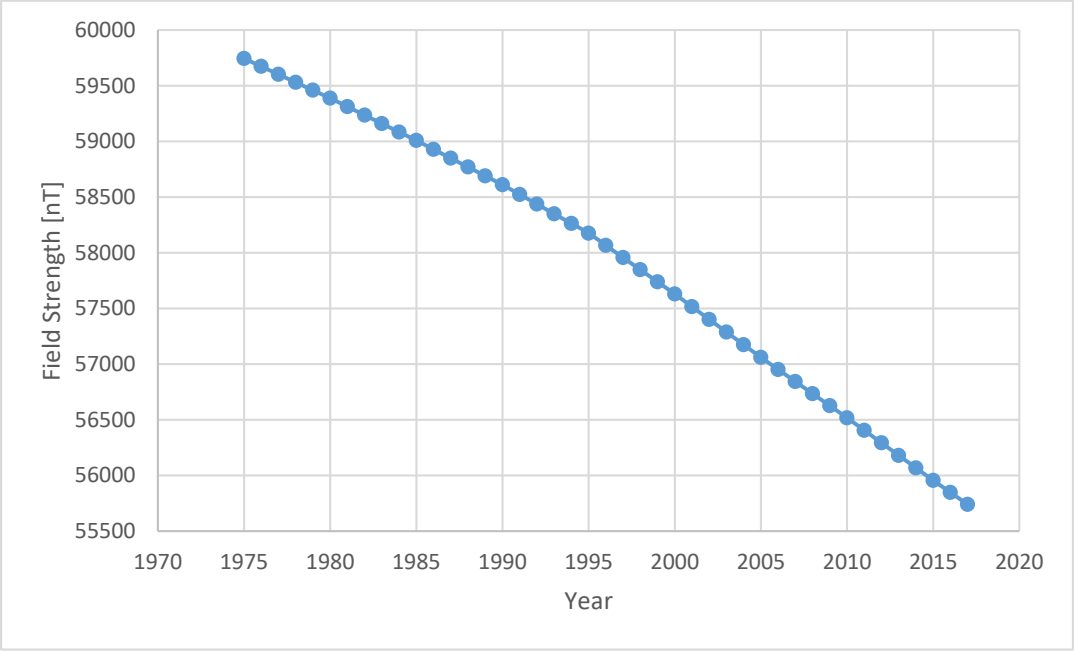

Figure 16 Plot of the change in magnetic field strength over time of the Interantional Geomagnetic Reference Field.

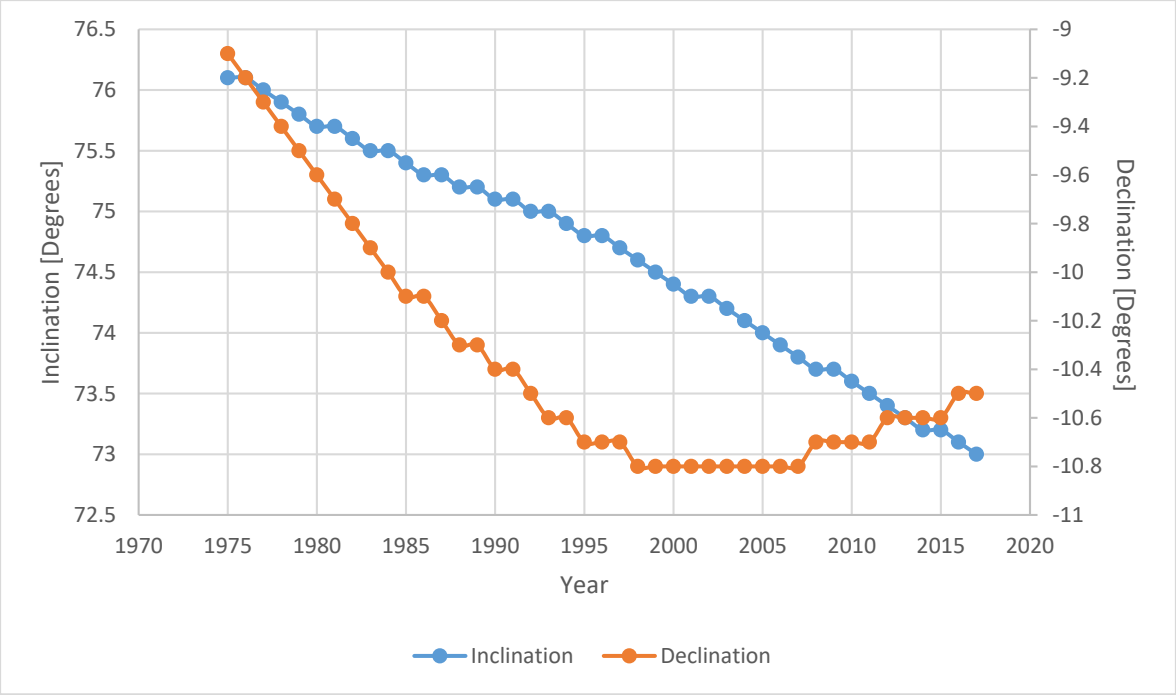

Figure 17 Plot of the change in inclination and declination over time of the International Geomagnetic Reference Field.